

ANISOTROPIC GEODESIC FILTER FOR SPECKLE NOISE REDUCTION AND EDGE  
PRESERVATION IN 2D AND 3D ECHOCARDIOGRAPHY

by

**Nehan Khan**

A thesis submitted in partial fulfillment of the requirements for the degree of

**Master of Science**

Department of **Computing Science**  
**University of Alberta**

©Nehan Khan, 2018

# Abstract

It is a challenge today for medical practitioners and manufacturers to improve ultrasound image quality as the technology has reached its physical limits. Ultrasound images are a great help for non-invasive diagnostics but suffer from a wide variety of artifacts such as shadowing, limited field of view, and speckle noise. The main focus of this thesis is on the application of a new non-linear image processing technique in cardiac ultrasound imaging and more specifically on various methods to reduce multiplicative speckle noise. Various filtering techniques for speckle noise reduction have been proposed in the past; however, their performances are still limited as a compromise between speckle noise reduction and image features preservation is difficult to reach.

In this thesis, an anisotropic geodesic filtering algorithm is proposed to reduce the multiplicative noise in cardiac ultrasound images. The algorithm is based on a scale-space filtering technique comparable to Gaussian filtering but with the difference that the Gaussian weights are automatically modified using a non-linear geodesic distance calculation between the pixels which is capable of automatically preserving edges. In the thesis, the proposed anisotropic geodesic filter is compared to various existing filters such as Gaussian filter, median filter, and other types of non-linear filters based on gradient-based anisotropic diffusion. We demonstrate that the proposed anisotropic geodesic filter performs best in terms of preserving features and at the same time can provide improvements to the signal-to-noise-ratio of real-time 2D and 3D echo-cardiographs. The proposed algorithm is validated on real-world ultrasound images comparing signal-to-noise-ratio (SNR), root-mean-square-error (RMSE), peak-signal-to-noise-ratio (PSNR), contrast and contrast-to-noise-ratio (CNR).

## Dedication

This thesis is dedicated lovingly to my husband, Ahmed Mohammed and our beloved son, Arhaan Ahmed. I would also like to dedicate this to my parents, whose support, encouragement and constant love have sustained me throughout my life.

# Acknowledgements

I would like to express my deepest gratitude to my supervisors Dr. Pierre Boulanger and Dr. Kumaradevan Punithakumar for their unwavering support, financial assistance, mentorship and last but not the least for giving me the opportunity to work on this project that has helped me learn so much more. I would also like to extend a warm thanks for the friendly learning environment that you have created in the SERVIER Virtual Cardiac Center.

I would especially like to thank Dr. Boulanger for sharing invaluable life experiences and for helping me through the process. He has provided constant guidance and also helped me develop my background in the field of medical imaging. A big thanks to Dr. Kumar for the long brainstorming session and for patiently correcting and supporting me whenever I needed help with various topics. I would also like to acknowledge and thank Dr. Abhilash Hareendranathan whose support, coaching, and companionship has been instrumental in overcoming several issues. I would also like to thank all the members of SERVIER Virtual Cardiac Center for their support.

I wish to acknowledge the people who mean a lot to me, my parents, Mohammed Rahimuddin Khan and Nasreen Khan, for showing faith in me and giving me the liberty to choose what I desired. My life achievements wouldn't have been possible without your unconditional love, endless support and belief. Thank you for always being there for me.

Finally, I owe thanks to a very special person, my husband, Ahmed Mohammed for his continued and unconditional love, support and understanding during my pursuit of this degree that made the completion of my thesis possible. You were always around at times I thought that it is impossible to continue, you helped me to keep things in perspective. I greatly value his contribution and deeply appreciate his belief in me. I appreciate my little guy, Arhaan for abiding my ignorance and the patience he showed during my thesis writing. Words would never say how grateful I am to both of you. I consider myself the

luckiest women in the world to have such a loving and caring family, standing beside me with love and support. I thank the Almighty Allah for giving me the strength and patience to complete my work and manage everything and stand proudly with my head held high.

I thank Servier Canada Inc. and the Heart and Stroke Foundation of Alberta, NWT & Nunavut for the research and funding that continues to support this work.

# Contents

<b>1</b>	<b>INTRODUCTION</b>	<b>1</b>
1.1	Motivations . . . . .	2
1.2	Ultrasound Noise Model . . . . .	3
1.3	Thesis Contributions . . . . .	5
1.4	Thesis Organization . . . . .	5
<b>2</b>	<b>LITERATURE REVIEW</b>	<b>6</b>
2.1	Ultrasound Imaging . . . . .	6
2.1.1	Types of Noise . . . . .	7
2.1.2	Reduction of Speckle Noise . . . . .	8
2.1.3	Homomorphic Filtering: . . . . .	13
2.1.4	Filters used for Comparison . . . . .	14
2.2	Conclusion . . . . .	16
<b>3</b>	<b>ANISOTROPIC GEODESIC FILTERING</b>	<b>18</b>
3.1	Geodesic Filter Algorithm . . . . .	18
3.1.1	Geodesic Distances or Geodesic Trajectories . . . . .	19
3.2	Filtering a 3D and 2D Ultrasound Images . . . . .	21
3.3	Conclusion . . . . .	22
<b>4</b>	<b>RESULTS AND ANALYSIS</b>	<b>23</b>
4.1	Image Data Set . . . . .	23
4.2	2D Ultrasound Filtering Results . . . . .	24
4.3	3D Ultrasound Filtering Results . . . . .	29
4.3.1	Quantitative Analysis . . . . .	35

4.3.2	Signal-to-Noise-Ratio . . . . .	35
4.3.3	Root-Mean-Square-Error: . . . . .	35
4.3.4	Peak-Signal-to-Noise-Ratio . . . . .	36
4.3.5	Image Contrast Changes . . . . .	36
4.3.6	Contrast-to-Noise-Ratio: . . . . .	37
4.4	Comparison Between the Four Algorithms . . . . .	37
<b>5</b>	<b>Conclusion and Future Work</b>	<b>41</b>
5.1	Future Work . . . . .	41
	<b>Bibliography</b>	<b>43</b>
	<b>Appendix A Matlab Code For 3D Geodesic Filter</b>	<b>48</b>

# List of Figures

1.1	Image acquisition using Siemens ACUSON SC2000 . . . . .	2
1.2	Block diagram of the proposed filtering approach . . . . .	4
2.1	Ultrasound technique for image acquisition . . . . .	7
2.2	2D ultrasound image . . . . .	7
2.3	Homomorphic filtering on a 2D phantom cardiac ultrasound image . . . . .	14
4.1	Gaussian filter with varying sigma for phantom cardiac ultrasound image .	24
4.2	Gaussian filter with varying sigma for volunteer cardiac ultrasound image .	25
4.3	Median filter with varying window size for phantom cardiac ultrasound image	25
4.4	Median filter with varying window size for volunteer cardiac ultrasound image . . . . .	26
4.5	PAMD with varying parameter for phantom cardiac ultrasound image . . .	26
4.6	PAMD with varying parameter for volunteer cardiac ultrasound image . . .	27
4.7	Proposed filter with varying sigma for phantom cardiac ultrasound image .	27
4.8	Proposed filter with varying sigma for volunteer cardiac ultrasound image .	28
4.9	Proposed filter with varying window size for volunteer cardiac ultrasound image . . . . .	28
4.10	Original cardiac phantom ultrasound. . . . .	29
4.11	Proposed 3D filter for the cardiac phantom ultrasound $\sigma = 5$ . . . . .	30
4.12	Original volunteer cardiac ultrasound . . . . .	30
4.13	Proposed 3D filter for volunteer cardiac ultrasound for $\sigma = 5$ . . . . .	31
4.14	Proposed 3D filter for volunteer cardiac ultrasound for window size = 3x3 .	31
4.15	Proposed 3D filter for volunteer cardiac ultrasound for window size = 5x5 .	32
4.16	Proposed 3D filter for volunteer cardiac ultrasound for window size = 7x7 .	32

4.17	Proposed 3D filter for volunteer cardiac ultrasound for window size = 11x11	33
4.18	Gaussian filter - volunteer cardiac ultrasound image for $\sigma = 5$	33
4.19	Median filter - volunteer cardiac ultrasound image for a window size of $5 \times 5$	34
4.20	PAMD - volunteer cardiac ultrasound image for diffusion time $T = 0.09$	34
4.21	Image showing region of interest for performing quantitative measurement analysis.	38

# List of Tables

4.1	<i>Metrics values for noisy image</i>	39
4.2	<i>Metrics values for Gaussian filtering with variable sigma; window size = 3x3</i>	39
4.3	<i>Metrics values for Gaussian filtering with variable sigma; window size = 11x11</i>	39
4.4	<i>Metrics values for Median filtering with variable window size.</i>	39
4.5	<i>Metrics values for Anisotropic Diffusion - gradient based with variable parameters.</i>	39
4.6	<i>Metrics values for Anisotropic Geodesic with variable sigma; window size = 3x3</i>	40
4.7	<i>Metrics values for Anisotropic Geodesic with variable sigma; window size =11x11</i>	40

# Chapter 1

## INTRODUCTION

In medical image processing, noise reduction still remains a challenge for researchers and clinicians. Reliable image processing methods for magnetic resonance imaging (MRI), X-rays tomography (CT), x-ray, and ultrasound (US) are essential to improve the diagnostic analysis and compensate for instrumental artifacts. The quality of medical images is determined by a number of factors which originates from the physical phenomenon measured by the sensors and by the reconstruction algorithms. The main challenge for developing different noise reduction techniques is to improve signal-to-noise ratio without losing important clinical features in the image. Over the past decades, several image processing techniques focusing on reducing multiplicative ‘speckle’ noise prevalent in ultrasound imaging has been proposed. A number of advances in data acquisition and sensors (See Figure 1.1) have improved the image quality of ultrasound but many of these advances have now reached their theoretical physical limits and most of the new image quality improvement is now coming from image post-processing. Image post-processing techniques do not require any sort of hardware modifications and can be applied to both old and new image data sets. **The compromise between the need to reduce multiplicative and additive noises in ultrasound images and the preservation of important image features represents a great challenge, which we will attempt to address in this thesis.** Several techniques for reducing ultrasound multiplicative and additive noises have been developed in the past and a majority of these filtering techniques fall in one of the three categories - local algorithms, anisotropic based techniques, and wavelet-based methods. We will discuss in detail each technique in the literature review.

In this thesis, a new approach using a non-linear anisotropic geodesic filtering technique

is presented. The concept of the filter was first proposed by Boulanger [1] for range image processing and is now being generalized to ultrasound imaging. In the thesis, we will compare the properties of this non-linear filter to various existing filters including the very popular Perona and Malik anisotropic diffusion (PAMD) filter [2]. This comparison will be achieved by measuring traditional distortion measures such as contrast-to-noise-ratio (CNR), signal-to-noise-ratio (SNR), mean-square error (MSE), peak signal-to-noise-ratio (PSNR), and correlation coefficients between reference images.

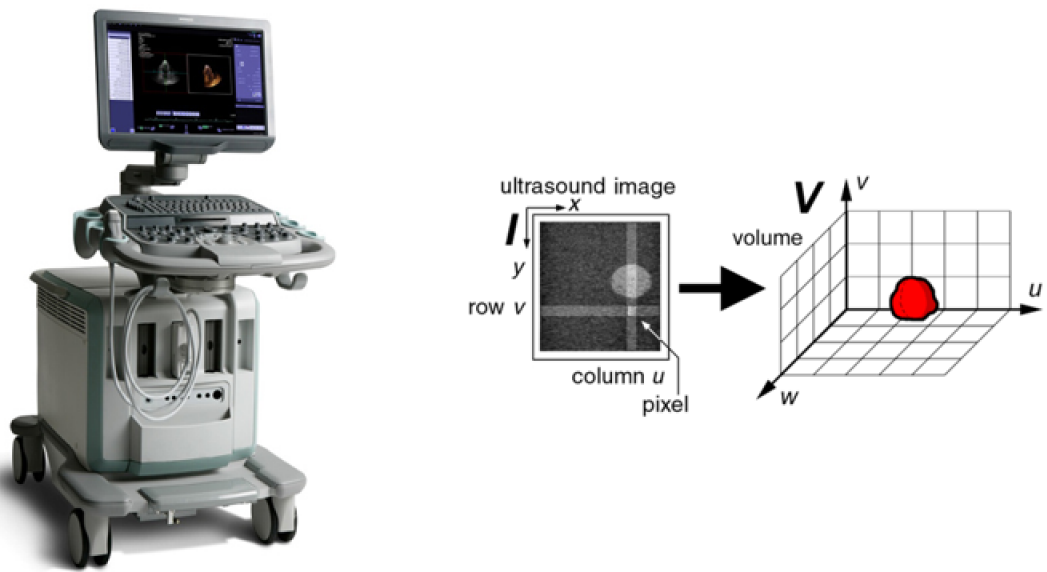


Figure 1.1: Image acquisition using Siemens ACUSON SC2000

## 1.1 Motivations

The last decade has seen an increase in cumulative patient radiation dose received from a wide variety of X-ray devices including classical X-ray, CT, interventional radiology, and mammography. The deleterious effects of larger doses of diagnostic radiation have received widespread coverage and have been documented in a large National Institutes of Health (NIH) study [3]. In order to resolve this problem a trend towards non-ionizing diagnostic imaging equipment, such as MRI and ultrasound imaging have been proposed. The utilization of ultrasound for general diagnostic imaging is appropriate because of its

non-invasive nature, speed, low-cost, safety, scanner portability, etc. On the other hand, ultrasound images are often low-contrast; they contain a lot of artifacts and noise. In addition, the noise in ultrasound images is difficult to reduce because of a combination of additive noise and speckle noise which is multiplicative in nature and is much more complicated to reduce than the typical Gaussian additive noise.

Noise reduction in medical ultrasound imaging is one of the most important post-processing steps in clinical settings in order to increase the signal to noise ratio and contrast. Various filtering techniques for speckle noise reduction have been proposed in the past; however, their performances are still limited as a compromise between speckle noise reduction and the preservation image features. A review of these methods will be presented in Chapter 2.

A good ultrasound image filter must have the following properties:

1. Must be able to deal with multiplicative noise such as speckle as well as additive noise;
2. Must be able to represent images at multi-scale without losing the localization of important features;
3. Must be computationally efficient.

## 1.2 Ultrasound Noise Model

It is not an easy task to filter volumetric ultrasound data since it is contaminated by additive and multiplicative noises at the same time. Speckle is basically a form of multiplicative noise that displays a granular pattern caused by the transducer. The distribution of speckle noise in ultrasound images has been largely studied in the literature and many models have been proposed. In this thesis, we use the noise model proposed by Loupas *et al.* [4] which is the most widely accepted and has been successfully used in many studies. The noise model is the following:

$$f(x, y, z) = g(x, y, z) \times \eta(x, y, z) + \beta(x, y, z),$$

where  $f(x,y,z)$  is a noisy ultrasound volumetric image,  $g(x,y,z)$  is the noise-free ultrasound volumetric image,  $\eta(x,y,z)$  and  $\beta(x,y,z)$  are the multiplicative and additive noise respectively. The additive noise  $\beta(x,y,z)$  is assumed to follow a Gaussian distribution with variance  $\hat{\sigma}(x,y,z)$  and an expected value  $E(\beta(x,y,z)) = 0$  in all directions. In this framework, the expected value  $E()$  of the difference between the measured volumetric image and the contribution from the multiplicative noise is equal to the expected value of the additive noise and is assumed to be equal to zero:

$$E(f(x,y,z) - g(x,y,z) \times \eta(x,y,z)) = E(\beta(x,y,z)) = 0.$$

Therefore, it seems logical to transform the original measured ultrasound images with a logarithmic function, where the multiplicative speckle noise becomes additive:

$$\log[f(x,y,z)] = \log[g(x,y,z)] + \log[\eta(x,y,z)].$$

In order to respect this condition one must first filter  $f(x,y,z)$  using some non-linear filter capable of preserving key features and reducing the effect of additive noise and then perform a logarithm transform of the resulting image which is then filtered again with a similar filter to reduce multiplicative noise. An inverse log-function is then applied to the image produced by this second filter. One can see in Figure 1.2 the block diagram of the proposed filtering approach.

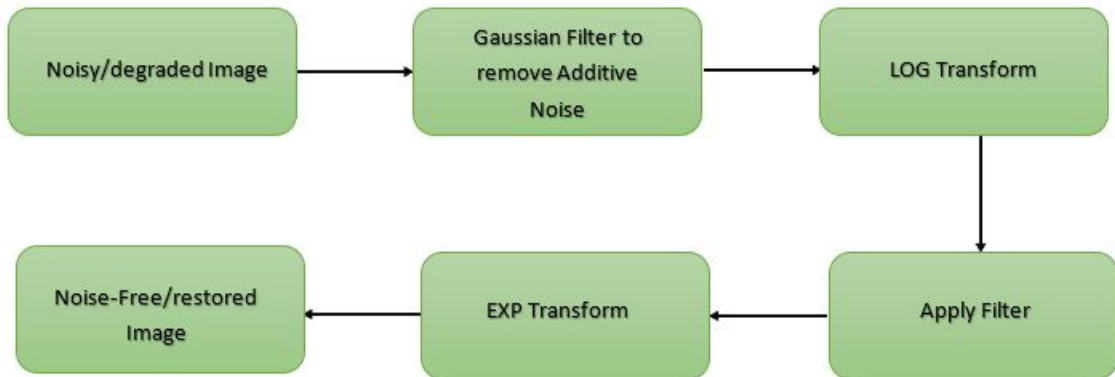


Figure 1.2: Block diagram of the proposed filtering approach

## 1.3 Thesis Contributions

The main contributions of the thesis are:

1. The development of a novel filter capable of reducing additive and speckle (multiplicative) noises in 2D and 3D ultrasound images without losing the localization of important features;
2. A new application of geodesic filters filtering technique to ultrasound image processing;
3. The ability to create a new multi-resolution scale space where edge localization is preserved;
4. An efficient algorithm to compute geodesic distances;
5. A quantitative comparison of the performance of the geodesic filter with three of the most popular filters found in the literature namely: Gaussian, median, and anisotropic diffusion filters.

## 1.4 Thesis Organization

The thesis is organized as follows. Chapter 2 reviews the history of ultrasound imaging as well as the physics of ultrasound image formation and the various type of noises found in those images. Another section in this chapter focuses on describing techniques to reduce speckle noise and also gives an overview of various filters used in our comparative analysis namely: Gaussian filter, median filter, and anisotropic diffusion gradient based filter. Chapter 3 describes the concept of geodesic filtering along with its properties and implementation. Chapters 4 discusses the qualitative and quantitative comparison with three of the most popular filters found in the literature. In Chapter 5, we conclude the thesis with the analysis of the pros and cons of the geodesic filter to perform speckle reduction in ultrasound images and discuss some possible future works and improvements.

# Chapter 2

## LITERATURE REVIEW

This chapter presents a brief history of ultrasound imaging and discusses the different noises associated with this modality as well as various techniques used to reduce its effect. Out of the numerous filters one can find in the literature, we will review the filters that will be used for the comparison with the proposed geodesic filter.

### 2.1 Ultrasound Imaging

Ultrasound is non-invasive imaging modality and one of the most inexpensive tools used for qualitative and quantitative assessments of patient's conditions. Ultrasound imaging technology is constantly and rapidly changing, ranging from cardiac imaging to pre-natal assessment. The use of ultrasound for medical imaging application is advantageous because it is safe to use, non-invasive in most applications and the image acquisition is real-time. Ultrasound imaging uses ultrasound waves produced from piezoelectric transducers that travel through the body tissues and/or organs which are then reflected back to receptors which turns ultrasound vibrations into electrical pulses where they are processed to compute the location of the reflected wave using time-of-flight. These transducers arrays are organized as 1D arrays or 2D arrays which produce respectively 2D or 3D images (see Figure 2.1). In general, the resolution of an ultrasound image varies with the number of elements in the transducer array and with the frequency of the ultrasound transducer used. In general, higher time resolution can be achieved when higher ultrasound frequencies are used but higher frequencies attenuate or are absorbed, faster than lower frequencies limiting the ability to observe deeper anatomical structures. Hence, there is a fundamental

physical limit between time resolution and depth penetration. In addition, other artifacts can be created by the loss of proper contact or a gap between the transducer probe and the body. This can be solved by using impedance adaptive gel that reduces the reflection of the ultrasound from the contact between air and skin.

Ultrasound images are degraded by an intrinsic artifact called “speckle”. Speckle is due to the fact that most surfaces are extremely rough on the scale of the wavelength which create interference of the returning wave at the transducer aperture. These scattered signals add coherently; that is, they add constructively and destructively depending on the relative phases of each scattered waveform. Speckle noise results from these patterns of constructive and destructive interference produce bright and dark dots in the image.

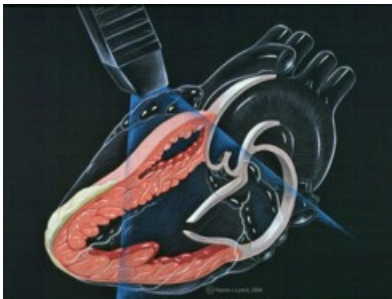


Figure 2.1: Ultrasound technique for image acquisition

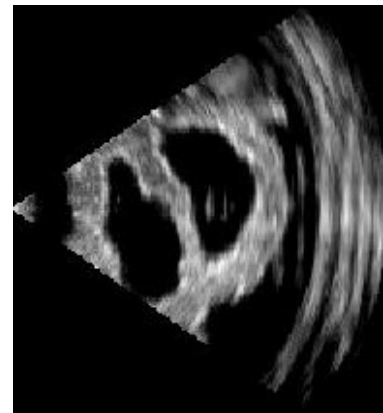


Figure 2.2: 2D ultrasound image

### 2.1.1 Types of Noise

There are different types of noise in digital images. These are impulse noise, additive noise, frequency noise, and multiplicative noise. Impulse noise can appear when one of the sensor element is saturated and or when the signal is lost. In this case, the image has too high or too low pixel value that creates outliers. Wide-band additive noise comes from many natural sources, such as the thermal vibrations of atoms in conductors, shot noise, black body, and amplifier gain variations. Additive noise follows simple statistical models such as Gaussian or normal distributions, and its effect can be reduced with linear filters. Frequency noise is characterized by the interference of a signal at specific frequencies, for example, 60 Hz noise created by the interference of a house electrical system with an instrument. Lastly,

multiplicative noise refers to an unwanted random signal that gets multiplied to a signal. For ultrasound imaging, speckle noise is multiplicative. In most ultrasound images, we have a combination of additive and multiplicative noises.

### **2.1.2 Reduction of Speckle Noise**

Speckle degrades the quality of ultrasound images and hence reduce the ability of a human observer to discriminate the fine details of diagnostic examination. Speckle is not a noise in an image but noise like variation in contrast. As mentioned previously, speckle noise is basically a form of multiplicative noise, which occurs when a sound wave pulse randomly interferes with the small particles or objects on a scale comparable to the sound wavelength. Speckle noise is defined as multiplicative noise, having a granular pattern it is an inherent property of an ultrasound image. Speckle is the result of the diffuse scattering, which occurs when an ultrasound pulse randomly interferes with the small particles or objects on a scale comparable to the sound wavelength.

Speckle reduction algorithms try to remove the speckle without destroying the important fine image features. Most of the past approaches for de-noising ultrasound images are based on non-adaptive and adaptive filtering techniques that will be discussed in the next section. However, it is well known that standard noise filtering methods often result in blurred image features. Images with speckle noise will result in reducing the contrast of an image and make it difficult to perform image processing operations like edge detection, segmentation, etc.

The problem of image smoothing is to reduce undesirable distortion due to the presence of noise or the poor image acquisition process that negatively affects image analysis and interpretation process, while preserving important features such as homogeneous regions, discontinuities, edges, and textures [5].

Speckle reducing filters are originated from the synthetic aperture radar (SAR) community [6]. Later, these filters were applied to ultrasound imaging since the early 1980s. The work of reducing or suppressing speckle noise in ultrasound going on for a long time now.

There are two major classifications of speckle reduction filters, namely single scale spatial filters and transform domain multi-scale filters. The spatial filter acts on an image by smoothing it; that is, it reduces the intensity variation between adjacent pixels. The simple sliding window spatial filter replaces the center value in the window with the average of all the neighboring pixel values including itself. By doing this, it replaces pixels, that are unrepresentative of their surroundings. It is usually implemented with a convolution mask which compute a new value for the central pixel as a weighted sum of the values of a pixel and its neighbors. If the coefficients of the mask normalized to one, then the average brightness of the image will not changed.

Several methods are used to eliminate speckle noise, based upon different mathematical models [4]. One method, for example, employs multiple-look processing, averaging out the speckle noise by taking several "view" at a target in a single ultrasound sweep [2][3]. The average is the incoherent average of the views [3].

A second method involves using adaptive and non-adaptive filters on the signal (where adaptive filters modify their weights across the image to the speckle level, and non-adaptive filters apply the same weights uniformly across the entire image). Such filtering also eliminates actual image information as well, in particular, high-frequency information such as fine anatomical features. Adaptive speckle filtering is better at preserving edges and detail in high-texture areas. Non-adaptive filtering is simpler to implement, and requires less computational power but unfortunately eliminate many of the important fine structures [2][3].

There are two forms of non-adaptive speckle filtering: one based on moving averages and one based upon the median (within a given rectangular window centered at a pixel). Median filter is better at preserving edges whilst eliminating noise spikes, than moving average filter such as the Gaussian filter. There are many forms of adaptive speckle filtering, including the Lee filter, the Frost filter, and the Refined Gamma Maximum-A-Posteriori (RGMAP) filter. They all rely upon three fundamental assumptions in their mathematical models[2]:

- Speckle noise is a multiplicative noise and is directly proportional to the local grey level in any area;

- The signal and the noise are statistically independent from each other;
- The sample mean and variance of a single pixel are equal to the mean and variance of the local area that is centred on that pixel;

In the following sections, we will review briefly some of the filtering algorithms proposed in the literature.

### **Wavelet Filter**

Recently, the use of wavelet transform has led to significant advances in filtering ultrasound images. The main reason for the use of multi-scale processing is the fact that many natural signals, when decomposed into wavelet bases are significantly simplified and can be modeled by known distributions. Besides, wavelet decomposition is able to separate noise and signal at different scales and orientations. Therefore, the original signal at any scale and direction can be recovered and useful details are not lost.

The first multi-scale wavelet speckle reduction methods were based on the thresholding of detail sub-band coefficients [8]. These algorithms are based on the observation that wavelet coefficients in each spectral band (the so-called VW, WV and WW blocks) can be modeled as a bi-Normal distribution of mean  $(V_x; V_y)$  (nearly zero) and covariance matrix  $\mathbf{R}$  which is in general not diagonal (real and imaginary parts are correlated). In addition, the distributions are usually oriented differently in each block. Based on this fact, an algorithm that performs wavelet coefficients thresholding with respect to the principal axes of the 2-D distributions. [8] [7].

Unfortunately, wavelet algorithms suffer from many limitations which makes their use in ultrasound image processing difficult.

- The choice of threshold is made in an ad hoc manner, supposing that signal and noise components obey their known distributions, irrespective of their scale and orientations;
- The thresholding procedure generally results in some artifacts in the de-noised image;
- To address these issues, non-linear estimators, based on Bayes theory have been developed;

### Kuan Filter

The Kuan filter [8] is based on a Minimum Mean Square Error (MMSE) criterion. A MMSE estimate is first developed for an additive noise model  $y = x + n$ . The multiplicative noise model is then considered under the form  $y = x + (n - 1)x$  from which a corresponding linear filter is deduced. The Kuan filter is optimal when both the scene and the detected intensities can be represented by a Gaussian distribution. Under the unit-mean noise assumption, the pixel value estimate  $\hat{x}$  is given by:

$$\hat{x} = \bar{y} + \frac{\sigma_x^2(y - \bar{y})}{\sigma_x^2 + (\bar{y}^2 + \sigma_x^2)/L} \quad (2.1)$$

$$\sigma_x^2 = \frac{L\sigma_y^2 - \text{bar}y^2}{L + 1}, \quad (2.2)$$

where  $\bar{y}$  is the mean of the neighbourhood,  $y$  is the measured pixel,  $\sigma_x$  the variance of  $x$  and  $L$  is defined as:

$$\left( \frac{\text{mean}}{\text{standard deviation}} \right)^2. \quad (2.3)$$

### Lee Filter

The Lee filter [9] converts the multiplicative model into an additive one, thereby reducing the problem of dealing with speckle noise to a known tractable additive noise problem. This filter is a particular case of the Kuan filter when the term  $\sigma_x^2/L$  is removed from Eq.2.1.

### Gamma Filter

The Gamma filter [10] is a Maximum A Posteriori (MAP) filter based on a Bayesian analysis of the image statistics. It assumes that both the scene reflectivity and the speckle noise follow a Gamma distribution. The "superposition" of these distributions yields a K-distribution which is recognized to match a large variety of radar return distributions. The estimate  $\hat{x}$  is given by:

$$\hat{x} = \frac{(\alpha - L - 1)\bar{y} + \sqrt{\bar{y}^2(\alpha - L - 1)^2 + 4\alpha L y \bar{y}}}{2\alpha} \quad (2.4)$$

$$\alpha = \frac{L + 1}{L(\sigma_y/\bar{y})^2 - 1} \quad (2.5)$$

### Forst Filter

The Frost filter [11] is an adaptive Wiener filter which convolves the pixel values within a fixed size window with an exponential impulse response  $m$  given by:

$$m = \exp [-KC_y(t_0)|t|] \quad C_y = \sigma_y/\bar{y} \quad (2.6)$$

where  $K$  is the filter parameter,  $t_0$  represents the location of the processed pixel and  $|t|$  is the distance measured from pixel  $t_0$ . This response results from an autoregressive exponential model assumed for the scene reflectivity  $x$ .

### Kalman Filter

A 2D Kalman filter [12] has been implemented on a causal prediction window, the so-called Non-Symmetric Half Plane (NSHP). In this filter, the image is assumed to be represented by a Markov Field which satisfies the causal autoregressive (AR) model

$$x(m, n) = \sum_{(p,q) \in W} a_{pq}x(m-p, n-q) + u(m, n) \quad (2.7)$$

where  $x(m, n)$  represents the pixel value at location  $(m, n)$ ,  $u(m, n)$  is a noise sequence (this is not the speckle noise) which drives the Markov process and  $a_{pq}$  are the reflection coefficients of the autoregressive model. The parameters  $a_{pq}$  are evaluated based upon the global estimates of the autocorrelation sequence of the image over the finite window  $W$ . From these parameters, the AR model can be arranged into a 2D block recursive form for the Kalman filter equations. Implementation of this filter is very much involved and we refer to [12] for more details about the 2D kinematic model (limited here to speckle modelling only) and the Kalman filter equation.

### Geometric Filter

The geometric filter [13] is a nonlinear morphological filter that uses the concept of image graph. The image graph is obtained by transforming the original image into a 3-dimensional diagram where the pixel coordinates specify the position of the pixel on a plane and the pixel value specifies the elevation of the pixel with respect to that plane. The filtering process itself is performed first on row slices of the image graph using a 8-hulling

algorithm. Slice pixels are set to 1 if the pixel is on or below the image graph surface, while pixels above the image graph surface are set to 0. The filtering algorithm searches for 4 different configurations ( $(3 \times 3)$  binary morphological masks) and when it finds one, the graph pixel corresponding to the central pixel of the mask is set to 0. The procedure is repeated for the complementary graphs and masks except that the central pixel is now incremented by 1. The whole procedure is repeated on column and diagonal slices. This completes one iterative step of the geometric filter. A filtering is achieved because speckle appears as narrow walls and valleys on the binary slice images and because the geometric filter, through iterative repetition, gradually tears down and fills up these features.

### **Oddy Filter**

The Oddy filter [14] can be considered as a mean filter whose window shape varies according to the local statistics. This filter is the closest to the one proposed in this thesis. The estimate  $\hat{x}$  is given by:

$$\hat{x} = \bar{y} \text{ if } m < \alpha\bar{y} \quad \hat{x} = \frac{\sum_k \sum_l W_{kl} y(k, l)}{\sum_k \sum_l W_{kl}} \text{ if } m > \alpha\bar{y}$$

$$W_{kl} = 1 \text{ if } |y(k, l) - y| < m \quad W_{kl} = 0 \text{ otherwise,} \quad (2.8)$$

where  $\hat{x}$  is evaluated locally over a  $3 \times 3$  window,  $m = 1/8 \sum_k \sum_l |y(k, l) - y|$  and  $\alpha$  is the filter parameter.  $W$  plays the role of an adaptive binary mask that is applied over the window.

### **AFS Filter**

AFS filter [15] stands for Adaptive Filter on Surfaces. It is another adaptive mask filter that uses the concept of “local emerging surface” (l.e.s.) value. The l.e.s. is the area of the image graph surface defined over the window. The l.e.s. is calculated for the 9 binary masks. The mask whose l.e.s. is a minimum is selected and a mean filtering is performed over the mask pixels. The mean value is assigned to the central pixel of the  $5 \times 5$  window.

## **2.1.3 Homomorphic Filtering:**

Speckle noise present in ultrasound images is considered multiplicative noise. This fact creates gaps in the previous methods since they are created, mainly, to eliminate random

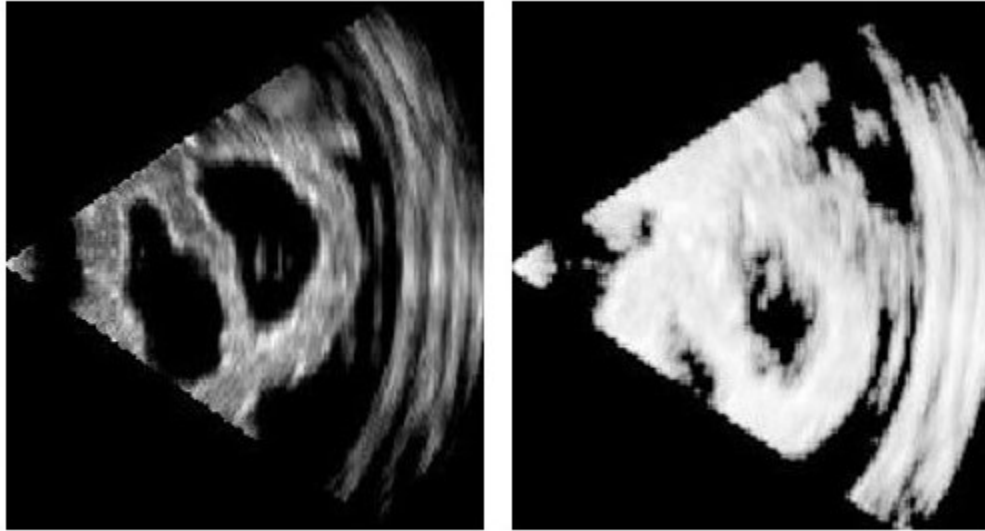


Figure 2.3: Homomorphic filtering on a 2D phantom cardiac ultrasound image

noise which occurs additively. Therefore, it seems logical to carry out a logarithmic transform on the original image, wherefore speckle noise becomes additive as is shown in the following equality:

$$\log[f(x, y, z)] = \log[g(x, y, z)] + \log[\eta(x, y, z)]$$

We now have an image without multiplicative noise which can be processed by traditional methods. At this point, we can choose from several options, one of the most common being the application of various convolution filters. In order to compare the proposed algorithm to the most common filters in the homomorphic context we will review: Gaussian filter, median filter, and Anisotropic Diffusion - Gradient based Filter. A description of each filters follows.

#### 2.1.4 Filters used for Comparison

##### **Gaussian Filter:**

Gaussian filter is a filter whose impulse response is a Gaussian function (or an approximation to it). The Gaussian has the unique ability not to create new edges as its scale (standard deviation) is increased. This property enables the extraction of edges that represent different levels of details in an image. As the scale is increased, the number of extracted weak

and false edges are reduced. However, this results in edges shifting from their real or true positions and the amount of shift an edge makes not only depends upon the scale of the Gaussian filter but also the intensity distributions underlying the image. Mathematically, Gaussian filters modifies the input signal by convolution with a Gaussian function(the kernel is based on the Normal distribution curve), which tends to produces good results in reducing the noise and smoothing out the image. The 2-D version of the Gaussian distribution, with standard deviation  $\sigma$  for image  $I(x, y)$  is given by

$$Gauss[I(x, y)] = \frac{1}{\sigma\sqrt{2\pi}} \exp -\frac{(x^2+y^2)}{2\sigma^2}$$

### **Median Filter:**

A median filter is a powerful non-linear filter. It is mainly used in the photographic application, which changes the image intensity mean value if the spatial noise distribution in the image is not symmetrical within the window and also removes the pulse or spike noise[5]. Median filter is similar to the averaging filter except that the center pixel is replaced by the median value of all pixels in the window neighbourhood. Due to one of it property it is used to reduce impulse noise. Its main advantage is it preserves edges localization. Its main disadvantage is that extra time is needed for computation of the median value by sorting N pixel in the window. Its computational complexity is  $O(N\log N)$ .

### **Anisotropic Diffusion - Gradient Based Filter:**

The anisotropic filter starts with a generalized non-homogeneous partial difference equation simulating the physics of a diffusion process[2,30]

$$\frac{\partial f}{\partial t} = \nabla \cdot (D(|\nabla f|) \nabla f) + \alpha S$$

where  $f = f(x, y, z, t)$  is the image at a time  $t$  in the diffusion process with the initial condition,  $f(x, y, z, 0)$  representing the original noisy image,  $S = s(x, y, z, t)$  is a source term added to generalize the original diffusion equation and alpha is simply a weighting factor.

$S$  is usually derived from  $f$ .  $\nabla$  is the gradient operator with respect to spatial coordinates  $(x, y, z)$ .  $D()$  is a diffusion constant dependent on the local gradient.

At a steady state of the process, the functions (i.e., the solution of this equation with the

initial state being the noisy image) represents the smoothed image. The diffusion process can be controlled via the diffusion constant. The process will be isotropic when  $D()$  is a constant, i.e., diffusion occurs in all radial directions in the same rate. For speckle reduction in ultrasound, we use anisotropic diffusion where  $D()$  is a function of the gradient. In this way, the diffusion is dependent on whether there is an edge or not.  $D()$  define both the smoothing and the edge preserving aspects of the process. Common functions of  $D()$  are given below ( $k$  being constant).

$$\frac{\partial f}{\partial t} = \nabla \cdot (D(|\nabla f|) \nabla f) + \alpha S$$

For practical implementation, the diffusion equation needs to be discretized. This results in an iterative filtering operation. Based on a suitable criterion, the final filtered image is obtained after a number of iterations. Anisotropic filtering can also be combined with multi-scale decomposition (for example wavelet decomposition)[30]. This provides the additional ability to choose the diffusion process through scale dependent choice of  $D()$ .

**Pre- or post- Processing** Usually, medical ultrasound images are affected by the mixed noise, which is the combination of speckle noise and Gaussian noise. There are two factors that influence the usefulness of a smoothing filter. The first reduces the range of resolutions over which variations in the output appear by the filter variation  $w$ , in the frequency domain be small and second is increase in spatial localization by a small spatial variance  $x$ . So Gaussian filters are widely used in image filtering for removal of additive noise in the image before removal of speckle noise

## 2.2 Conclusion

Many filters have been proposed in literature for general image de-noising or image processing. Ultrasound images are corrupted by speckle, a specific noise which is associated with coherent imaging systems. Many algorithms have been proposed in the past decades to develop methods which are specific to ultrasound images.

Several authors have proposed different methods to solve this problem in the literature.

One of these methods consists of convolving image signals with Gaussian kernels of increasing size (scale) and then analyzing the evolving of signal features along the scale dimension. Adaptive smoothing, instead of Gaussian smoothing has been proposed to ease the interpretation of scale-space representations. The general idea behind adaptive smoothing is to apply variable convolution kernels, whose supports and shapes vary with the local properties of the signal to be smoothed. An overview of the adaptive filters can be found in [16, 17].

As reviewed in this chapter there are several adaptive filters in literature which are proposed to achieve a better result by varying window size and also preserve the feature like edges. Filters that have adaptive nature include Lee, Frost, Kuan, Enhanced Frost [18], and Enhanced Lee filter [18]. One of major problems in applying all of these algorithms to ultrasound image analysis is that the weight used to compute the pixel similarities in a neighbourhood are all based on ad-hoc functions. As a consequence, linear methods, which use fixed weights in the convolution kernel, are not suitable because it assumes that the neighbouring pixels come from a smooth distribution where only geometric distance from the central pixel is important. What is needed is a convolution kernel whose coefficients are locally established as a function of a non-linear geodesic distance transform that measure the true distance between the central pixel with its neighbours in space and in intensity, which is the basis of this thesis.

## Chapter 3

# ANISOTROPIC GEODESIC FILTERING

This thesis proposes a new approach to perform noise filtering for speckle reduction on 2D and 3D ultrasound images using an anisotropic geodesic filter. Anisotropic geodesic filtering is a Gaussian like filter, where as opposed to standard Gaussian filtering with fixed weight values are used, the weights are determined by the local geodesic distances computed from the cumulative spatial and intensity distances of the neighboring pixels with the center pixel inside a convolution window. In this scheme each convolution window is different and can adapt to local intensity and geometry variations. As will be demonstrated, this category of filter can preserve the localization of fine structures automatically without prior knowledge of the locations of intensity discontinuities and without the need to compute gradients like in Perona's algorithm [2]. The filter is a new application of an older concept developed during Boulanger's PhD thesis [1] where he used a similar filter to perform multi-scale analysis of range image using Gaussian and mean curvatures.

### 3.1 Geodesic Filter Algorithm

As mentioned previously the proposed algorithm is similar to Gaussian filtering but can adapt to local intensity and geometry variations. Similar to standard Gaussian filtering the filter can produce a multi-resolution scale-space representation with very interesting properties such as edge or boundary preservation. Let us now discuss in more details the geodesic filter.

In the original concept [1] range images were a sampled set of 3-D measurements corresponding to a surface observed from a particular sensor viewpoint. In this case, the range data  $\vec{r}$  is represented by a manifold function  $\vec{r} = \vec{f}(u, v)$  where  $\vec{r} = (x, y, z)^T$  is the coordinates of the range data relative to the sensor pre-defined coordinate system. In a similar way one can define an ultrasound image as a 4-D manifold defined by  $\mathbf{s} = (x(u, v), y(u, v), z(u, v), I(u, v))^T$  where  $\mathbf{s}(u, v)$  is the intensity and location of reflected sound wave which we will name geometry-intensity manifold.

In the algorithm proposed for this thesis, a distance measurement between a reference point  $\mathbf{p}$  and a neighbor point  $\mathbf{q}$  on a the 4-D manifold  $\mathbf{s}(u, v)$  must be calculated. Using this distance one can define a new filter:

$$G_\sigma * I(u, v) = \frac{1}{N_\sigma} \int_{-\infty}^{\infty} \int_{-\infty}^{\infty} \exp\left(-\frac{d_s^2(\mathbf{p}, \mathbf{q})}{2\sigma^2}\right) I(u - \tau, v - \xi) d\tau d\xi \quad (3.1)$$

where  $d_s$  represents the geodesic surface distance between two points on the 4-D manifold with parametric coordinates  $\mathbf{p} = \mathbf{s}(u, v)$  and  $\mathbf{q} = \mathbf{s}(u - \tau, v - \xi)$  respectively, and  $N_\sigma$  is a normalization factor defined by:

$$N_\sigma = \int_{-\infty}^{\infty} \int_{-\infty}^{\infty} \exp\left(-\frac{d_s^2(\mathbf{p}, \mathbf{q})}{2\sigma^2}\right) d\tau d\xi. \quad (3.2)$$

The parameter  $\sigma$ , as with a standard Gaussian filter, controls the size of the filtering operator. The following properties make such an filtering operator attractive:

- Its effect on a 4-D manifold is independent of the measurement orientation;
- It behaves as an anisotropic filter that performs adaptive smoothing on the manifold but does not require prior determination of discontinuities.

To explain this filter in detail, we will first explain the definition of geodesic distance or geodesic trajectories and then present how to compute the geodesic distance using a single source shortest path algorithm that was developed for the purpose of this thesis.

### 3.1.1 Geodesic Distances or Geodesic Trajectories

An interesting geodesic metric is defined by considering the actual length of the minimal paths defined on the 4-D manifold. The generalized geodesic distance  $d_s(\mathbf{p}, \mathbf{q})$  between

two points  $\mathbf{p}$  and  $\mathbf{q}$  on the geometry-intensity manifold is defined as the shortest length  $L_s$  of all the paths linking  $\mathbf{p}$  to  $\mathbf{q}$  on the manifold. These geodesics trajectories maybe called minimal paths since the sum of the grey-levels and the spatial distances along these paths is minimum. Let us now discuss how to compute these geodesic trajectories and distances.

**Algorithm to Compute Geodesics Trajectory using Single-Source Shortest Path Algorithm**

To obtain geodesic distances from the center point of a convolution window to its neighboring points, one needs to find a minimum trajectories from the center point to all other points in the window. We know from [1] that the manifold distance  $d_s$ , namely the minimum distance among all trajectories  $\mathbf{d}(u(\alpha), v(\alpha))$  joining the two points  $\mathbf{p}(u, v)$  and  $\mathbf{q}(u-\tau, v-\xi)$  is defined by:

$$d_s(\mathbf{p}, \mathbf{q}) = \min_{\alpha} s_{\alpha}(\mathbf{p}, \mathbf{q}) \tag{3.3}$$

where  $s_{\alpha}(\mathbf{p}, \mathbf{q})$  is the cumulative arc-length between the two points for a trajectory  $\alpha$  joining them on the manifold.

Note that the value of  $d_s$  will be large if the minimum trajectory goes across for example an intensity discontinuity. From the above equation, one can design an efficient algorithm to compute the geodesic distances by using the Single-Source Shortest Paths Algorithm for weighted graphs [19].

The vertices of the graph correspond to the points in the convolution window and the edges represent neighboring connections of points. For example, the discrete arc length of the edges between points  $\mathbf{p}(u_i, v_j)$  and  $\mathbf{q}(u_{i+1}, v_j)$  is given by:

$$\sqrt{\|\mathbf{d}(u_i, v_j) - \mathbf{d}(u_{i+1}, v_j)\|^2}. \tag{3.4}$$

The algorithm to find the minimum distances is given as follows:

**Input:**  $G = (V,E)$  (a weighted graph) and  $v$  (the source vertex corresponding to the center point)

**Output:** for each vertex  $w$ ,  $w.sp$  is the length of the shortest path from  $v$  to  $w$  and corresponding minimum trajectories  $w.tr$

```

begin
for all vertices  $w$  do
    /* $w$ .mark indicates if the vertex distance is determined*/
     $w$ .mark := false;
     $w$ .sp :=  $\infty$ ;
 $v$ .sp := 0;
 $v$ .tr := 0;
while there exists an unmarked vertex do
    let  $w$  be an unmarked vertex such that  $w$ .sp is minimum;
     $w$ .mark := true;
    for all neighboring edges  $(w,x)$  such that  $x$  is unmarked do
        if  $w$ .sp + length( $w,x$ )  $\leq$   $x$ .sp then
             $x$ .sp :=  $w$ .sp + length( $w,x$ );
             $x$ .tr :=  $w$ ;
end

```

In this algorithm, you need to find the minimum distances among a set of path lengths and to update the path lengths frequently. One can implement this efficiently by using a heap structure. All unmarked vertices are kept in a heap with their current known shortest path lengths from the center point  $v$  as their keys. To find an unmarked vertex  $w$  such that the path length  $w$ .sp is minimum, one can simply take it from the top of the heap. All the edges connected to the vertex  $w$  can be checked and the path lengths can be updated without difficulty. Since the elements of the heap are the vertices of the graph, the space requirement is only  $O(|V|)$ , where  $|V|$  denotes the number of vertices. The algorithm complexity is  $O((|E| + |V|)\log|V|)$ , where  $|E|$  denotes the number of edges.

## 3.2 Filtering a 3D and 2D Ultrasound Images

For a 3-D ultrasound represented by a voxel space  $V(i, j, m)$  each slice located at position  $z_m$  is represented by a 4-D manifold  $\mathbf{r}_m(i, j) = (x_m(i, j), y_m(i, j), z_m(i, j), \ln V(i, j, m))$ .

Equation 3.1 is reduced for each slice  $z_m$  to:

$$\hat{V}(i, j, m) = \exp \left( \frac{\sum_{k=-W/2}^{k=W/2} \sum_{l=-W/2}^{l=W/2} \ln(V(i+k, j+l, m)) \exp(-d^2(\mathbf{r}_m(i+k, j+l), \mathbf{r}_m(i, j)) / (2\sigma^2))}{\sum_{k=-W/2}^{k=W/2} \sum_{l=-W/2}^{l=W/2} \exp(-d^2(\mathbf{r}_m(i+k, j+l), \mathbf{r}_m(i, j)) / (2\sigma^2))} \right) \quad (3.5)$$

where the logarithmic transformation for the multiplicative noise case is included. For the 2D case, Equation 3.5 is simply when  $m = 1$ .

### 3.3 Conclusion

In this chapter, a novel filtering method to reduce speckle noise, based on geodesic calculation for two-dimensional and three-dimensional cardiac ultrasound is proposed. In the next chapter, we will demonstrate that the proposed filter can reduce speckle noise better than the three filters mentioned in literature review. We will demonstrate that it is a good choice to filter curves and edges in an ultrasound image as it preserves these features localization automatically. In the literature, the authors [33,41,45] have considered ultrasound images (natural/synthetic) with artificially added speckle noise content and have proposed methods for suppressing this speckle noise in such images. However, in this thesis, we use images measured by real ultrasound equipment which contain inherent speckle noise.

# Chapter 4

## RESULTS AND ANALYSIS

In order to demonstrate the performance of the new intrinsic filter, we performed a systematic comparison with the three well-known filter found in the literature: Gaussian filter, median filter, and Perona and Malik anisotropic filter. This comparison was achieved by measuring traditional distortion measures such as contrast-to-noise-ratio (CNR), signal-to-noise-ratio (SNR), mean-square error (MSE), peak signal-to-noise-ratio (PSNR), and correlation coefficients between reference images.

### 4.1 Image Data Set

For the purpose of this comparison, echocardiography scans from a cardiac ultrasound phantom with known dimension as well as six human volunteers were acquired using the Siemens ACUSON SC2000 ultrasound scanner by an expert sonographer. The protocol was approved by the Health Research Ethics Board of the University of Alberta and informed consent was obtained from all human volunteers included in the study. The first data set had a volume of  $196 \times 187 \times 172$  voxels with a voxel size of (0.85 mm x 0.85 mm x 0.73 mm) and the second data set was measured from six healthy volunteers which included parasternal and apical views of their heart. The number of volume data frames were 7 - 34 per cardiac cycle with a volumes size of  $137 \times 131 \times 120$  voxels with a voxel size of (0.74 mm x 0.74 mm x 0.63 mm). In order to reduce the presence of additive noise each volume slices were first filtered by a Gaussian filter of size  $5 \times 5$  with  $\sigma = 0.5$ .

## 4.2 2D Ultrasound Filtering Results

Let us look first visually at the evolution of a slice in both data sets as a function of each filter parameters. One can see at Figure 4.1 and 4.2 the evolution of the ultrasound slice images as a function of the parameter  $\sigma$  for the Gaussian filter and at Figure 4.3 and 4.4 the evolution of the same ultrasound slice images with median filters with window sizes from  $3 \times 3$ ,  $5 \times 5$ , and  $7 \times 7$ . As expected the Gaussian filter can reduce the speckle but at the expense of losing important features. On the other hand the median filter is capable of filtering the speckle without the loss of small feature when the window size is small but as the window increase the median filter loses fine image features like Gaussian filter. Figure 4.5 and 4.6 illustrate the evolution of the anisotropic diffusion filter with various diffusion time  $T$ . For this filter, one can see that the image get smoother with longer diffusion time without too much loss of small features. In Figure 4.7 and 4.8 one can see the result of the proposed geodesic filter. One can see that not only does the proposed filter reduce speckle noise as a function of  $\sigma$  but also preserves boundaries and fine features.

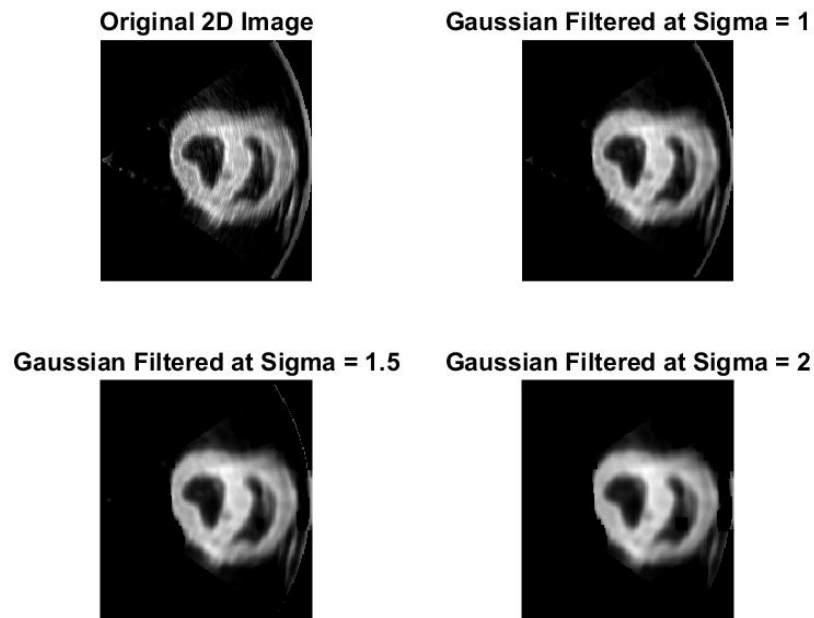


Figure 4.1: Gaussian filter with varying sigma for phantom cardiac ultrasound image

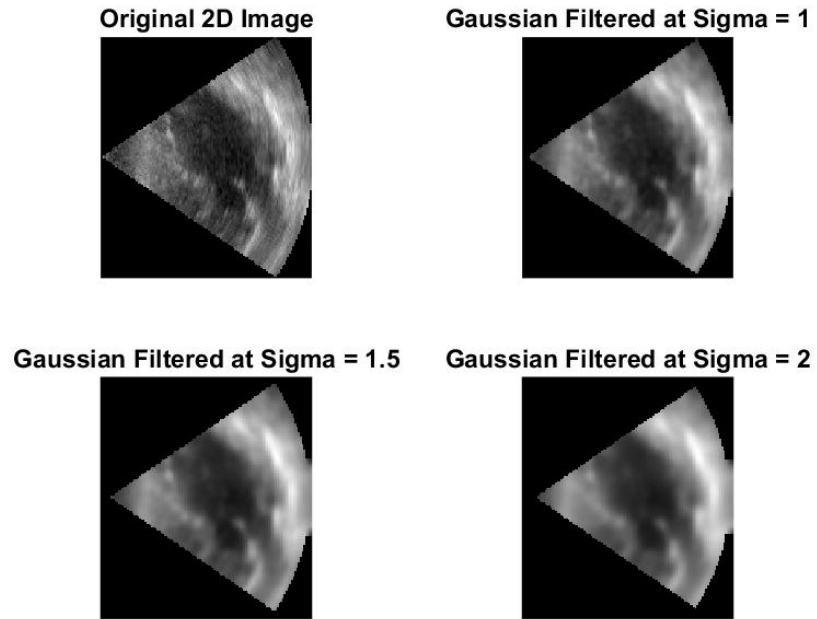


Figure 4.2: Gaussian filter with varying sigma for volunteer cardiac ultrasound image

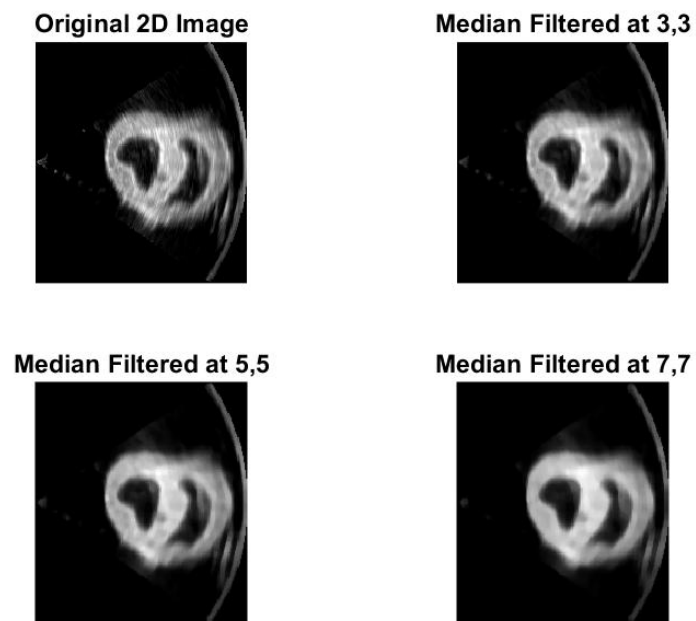


Figure 4.3: Median filter with varying window size for phantom cardiac ultrasound image

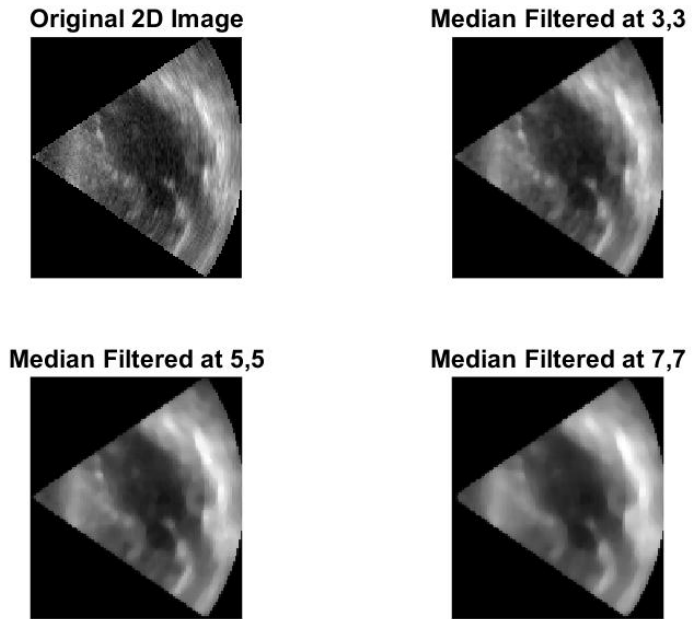


Figure 4.4: Median filter with varying window size for volunteer cardiac ultrasound image

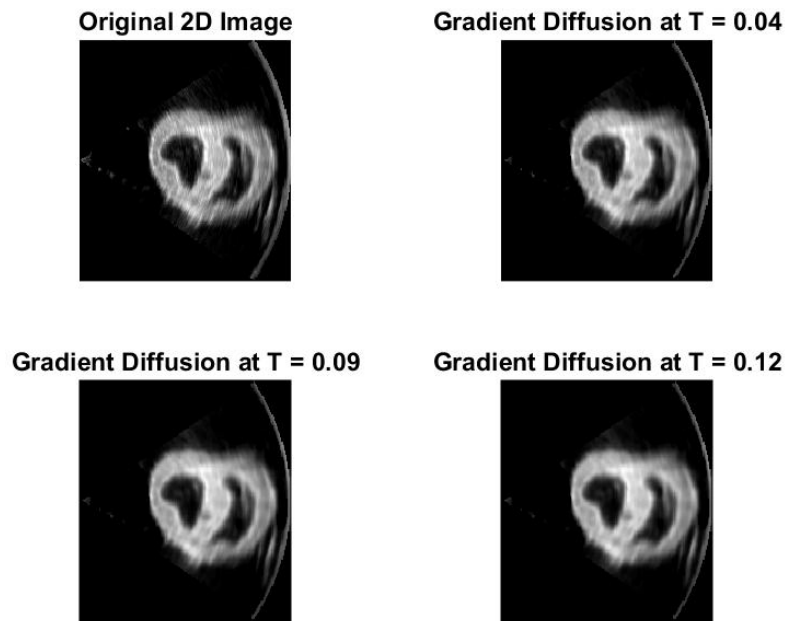


Figure 4.5: PAMD with varying parameter for phantom cardiac ultrasound image

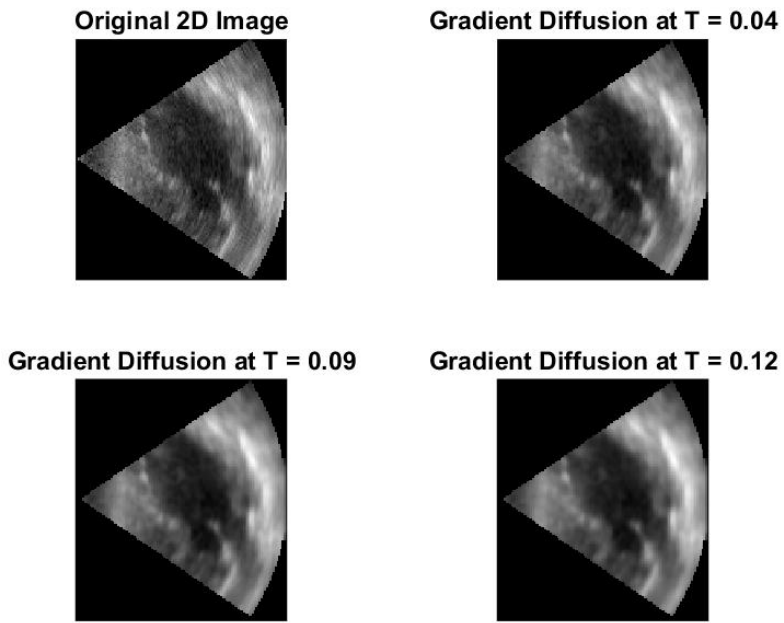


Figure 4.6: PAMD with varying parameter for volunteer cardiac ultrasound image

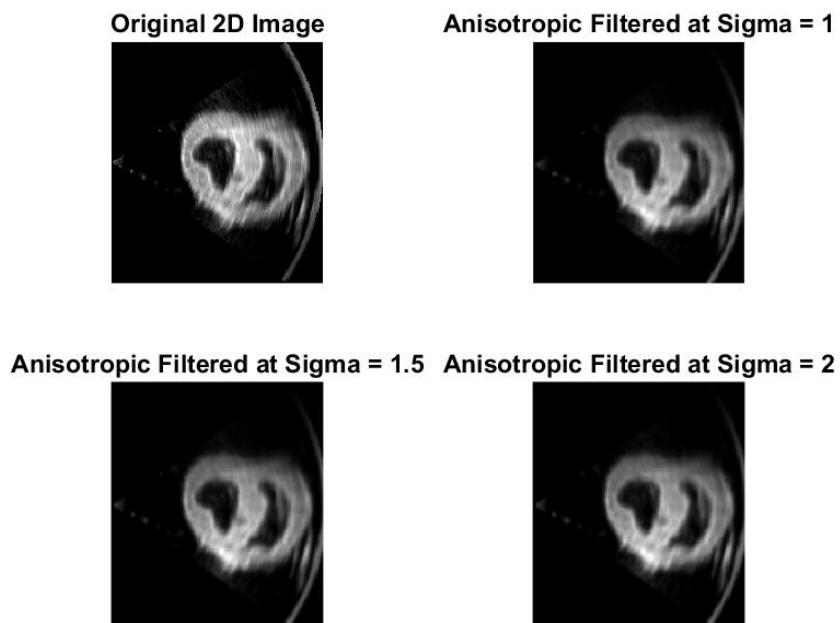


Figure 4.7: Proposed filter with varying sigma for phantom cardiac ultrasound image

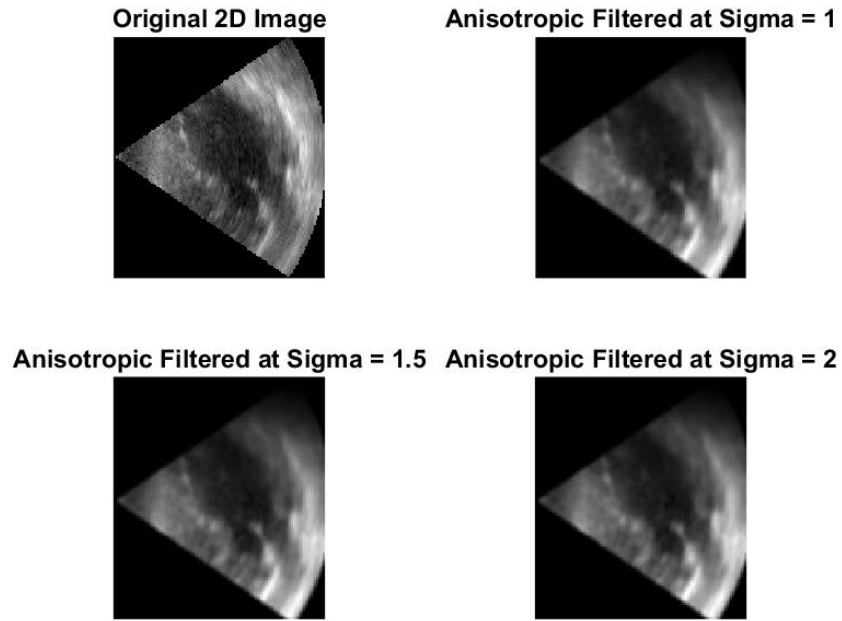


Figure 4.8: Proposed filter with varying sigma for volunteer cardiac ultrasound image

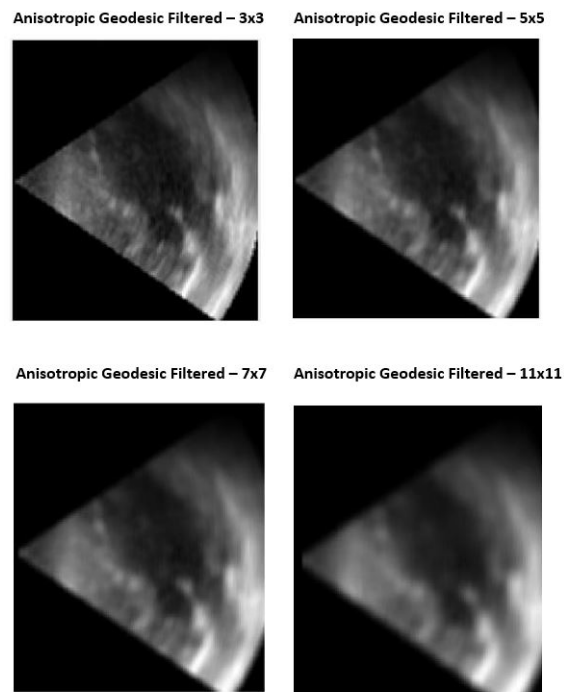


Figure 4.9: Proposed filter with varying window size for volunteer cardiac ultrasound image

### 4.3 3D Ultrasound Filtering Results

Before systematically comparing the results with the other filters, we would like to show for the different data sets results for the geodesic filter only. The 2D implementation of the geodesic anisotropic diffusion is extended to 3D as described in Chapter 3. The implementation of the filter was done in MATLAB and the vis3D function was used to display the 3D data set. One can see in the Figure 4.9 the original cardiac phantom data set in the YX-plane, YZ-plane, and XZ-plane as well as a combined 3D rendering. One can see in Figure 4.10 the filtered volume for  $\sigma = 5$ . One can see in the Figure 4.11 the original cardiac patient data. One can see in Figure 4.11 the filtered volume for  $\sigma = 5$ .

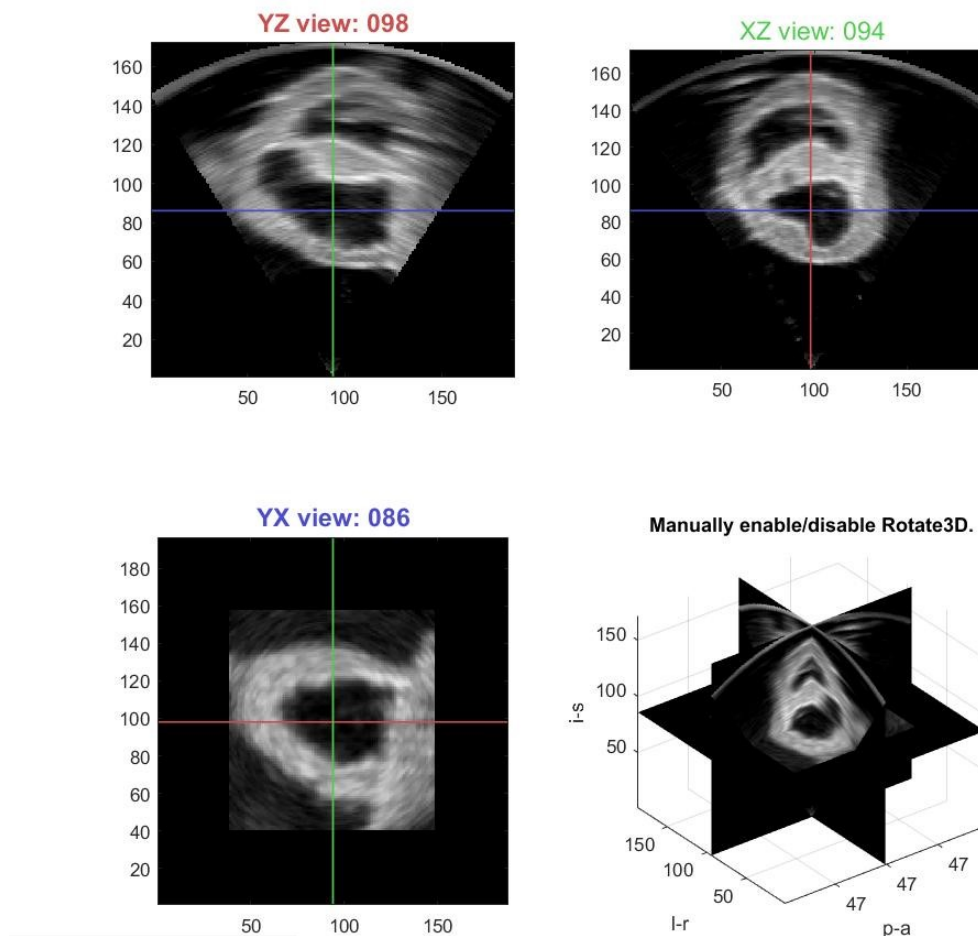


Figure 4.10: Original cardiac phantom ultrasound.

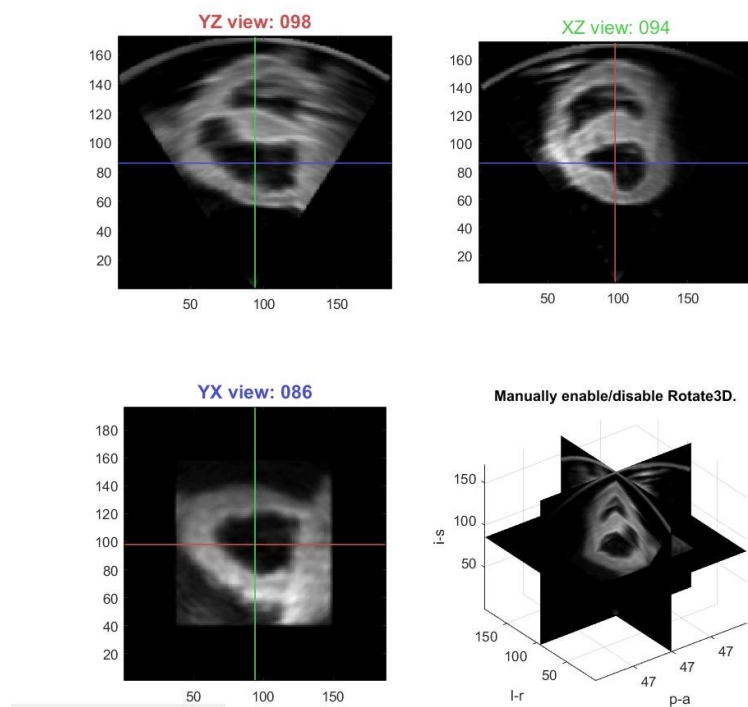


Figure 4.11: Proposed 3D filter for the cardiac phantom ultrasound  $\sigma = 5$

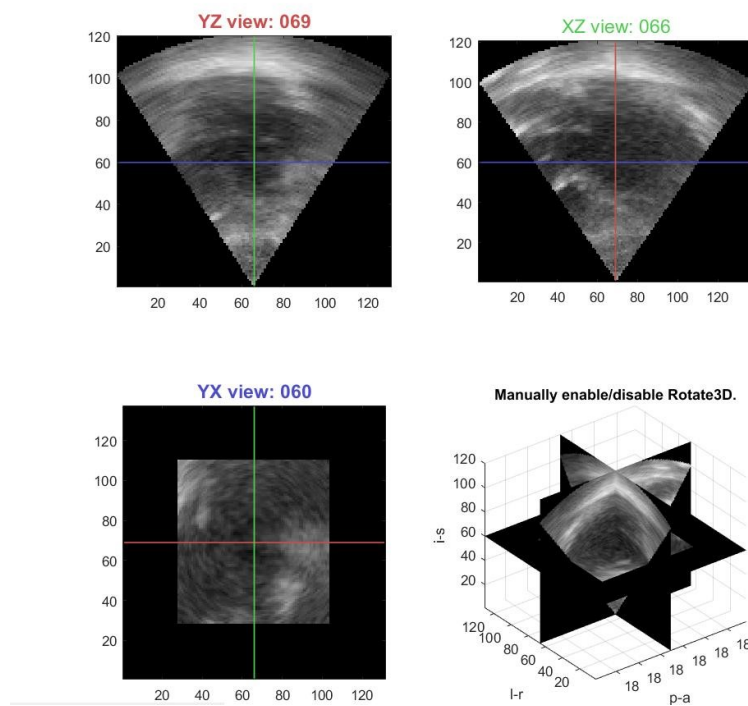


Figure 4.12: Original volunteer cardiac ultrasound

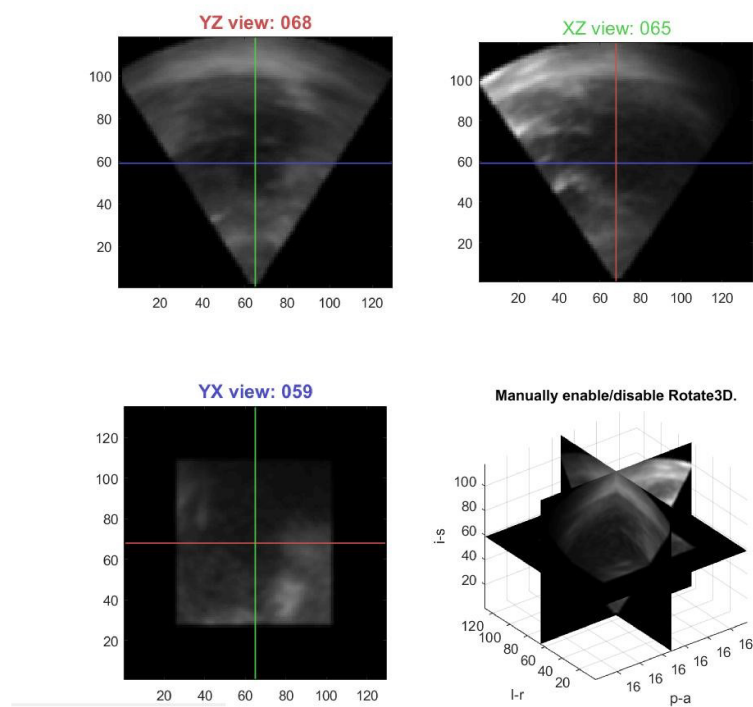


Figure 4.13: Proposed 3D filter for volunteer cardiac ultrasound for  $\sigma = 5$

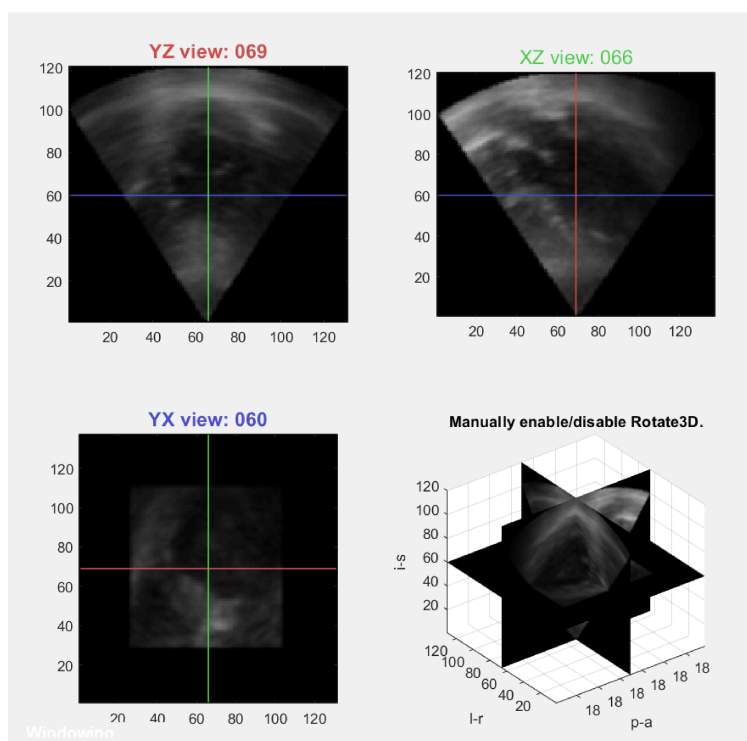


Figure 4.14: Proposed 3D filter for volunteer cardiac ultrasound for window size = 3x3

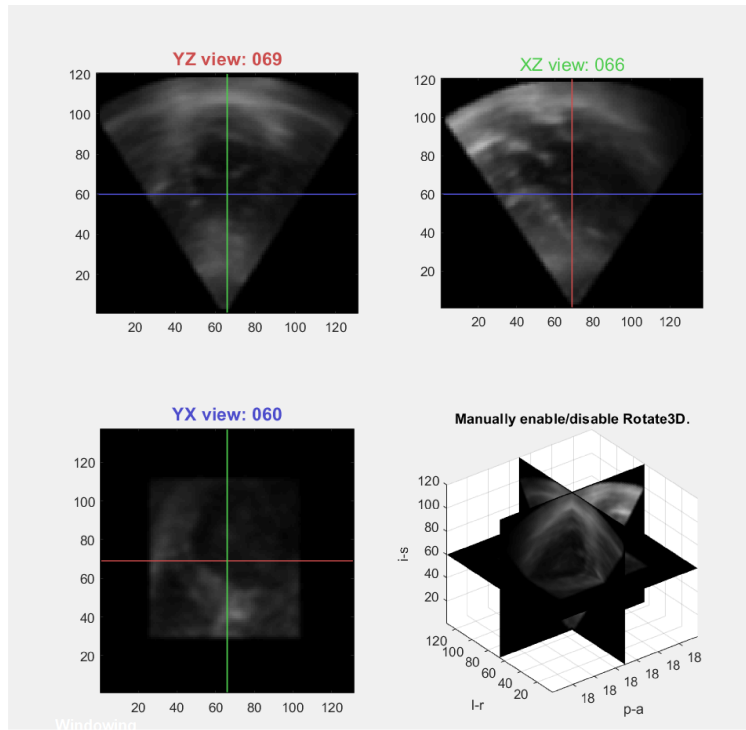


Figure 4.15: Proposed 3D filter for volunteer cardiac ultrasound for window size = 5x5

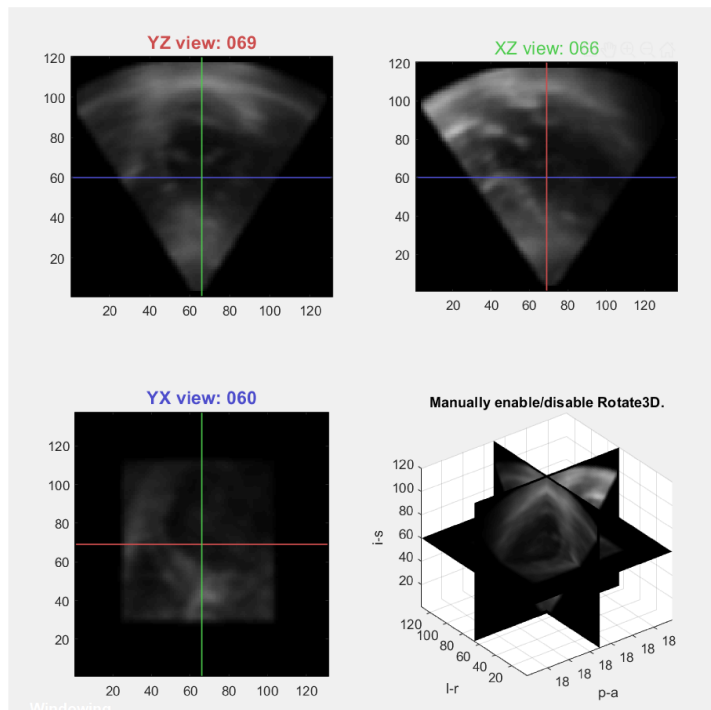


Figure 4.16: Proposed 3D filter for volunteer cardiac ultrasound for window size = 7x7

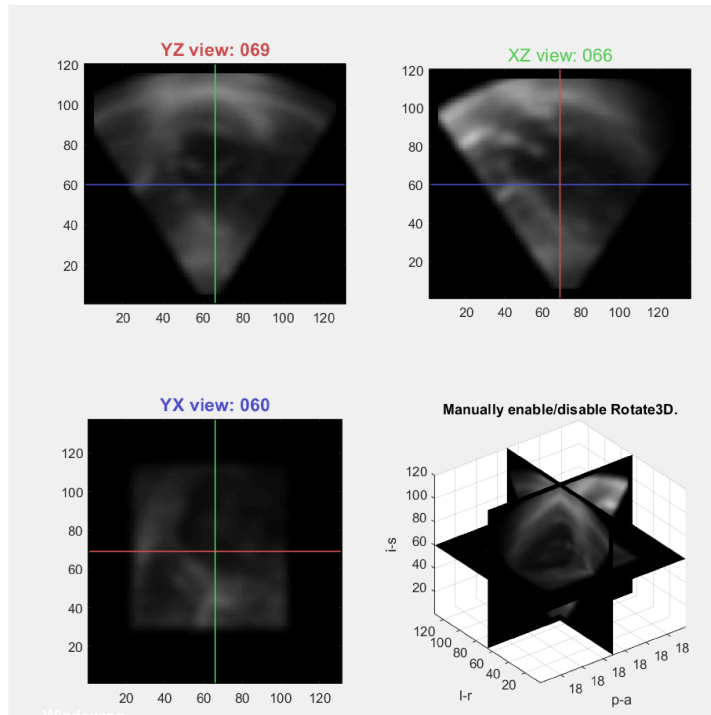


Figure 4.17: Proposed 3D filter for volunteer cardiac ultrasound for window size = 11x11

For visual comparison, one can see in Figures 4.18, 4.19, and 4.20 the filtering results for the three other methods.

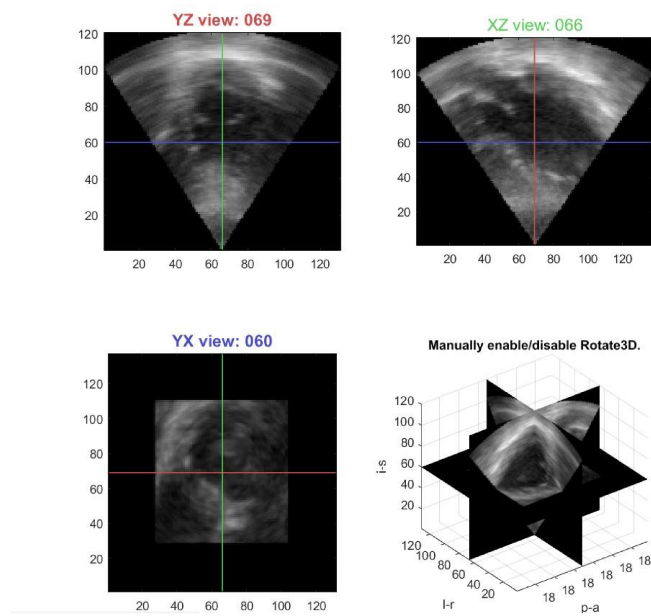


Figure 4.18: Gaussian filter - volunteer cardiac ultrasound image for  $\sigma = 5$

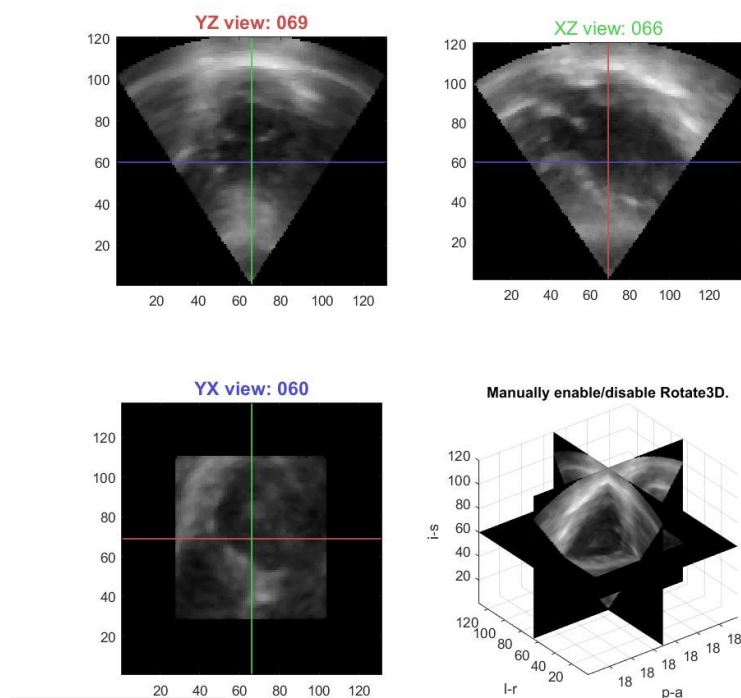


Figure 4.19: Median filter - volunteer cardiac ultrasound image for a window size of  $5 \times 5$

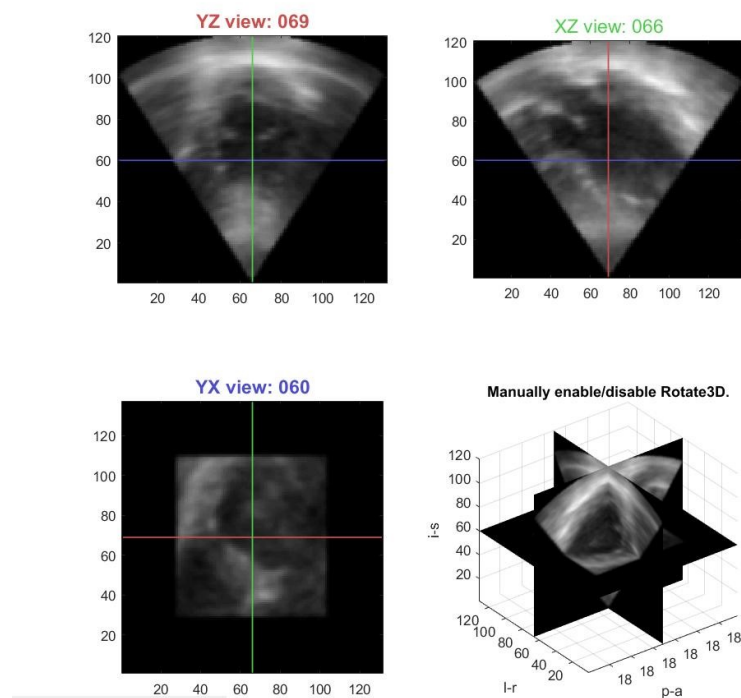


Figure 4.20: PAMD - volunteer cardiac ultrasound image for diffusion time  $T = 0.09$

### 4.3.1 Quantitative Analysis

This section describes a number of quantitative validation measures used to assess the quality of ultrasound images filtering using well known metrics such as: image contrast (IC), CNR, SNR, and PSNR. Lets first define those metrics mathematically and then study how the four filters compare to each other.

### 4.3.2 Signal-to-Noise-Ratio

For quantitative comparison, the SNR represents the ratio between the mean and the standard deviation values of the image pixel values within a region of interest, that is, the percentage of change in SNR,  $\Delta SNR$ , caused by filtering is defined as :

$$\Delta SNR = \frac{\Delta(SNR)^{my} + \Delta(SNR)^{bp}}{2}, \quad (4.1)$$

where  $\Delta SNR^{my}$  and  $\Delta SNR^{bp}$  denote the percentage of change in the SNR in the myocardial and blood-pool regions, respectively. The percentage of change in SNR in the myocardial region,  $\Delta SNR^{my}$ , is computed as:

$$\Delta(SNR^{my}) = \left[ \frac{\frac{\mu_f^{my}}{\sigma_f^{my}}}{\frac{1}{N} \sum_{i=1}^N \left( \frac{\mu_i^{my}}{\sigma_i^{my}} \right)} - 1 \right] * 100, \quad (4.2)$$

The percentage of change in SNR in the blood-pool region,  $\Delta SNR^{bp}$ , is computed in a similar way to  $\Delta SNR^{my}$ .

SNR is a good measure of speckle strength. The higher the SNR is , the less the speckle noise and the better the speckle reduction effect is. When SNR is measured it is taken as the average between the myocardial and blood-pool regions.

### 4.3.3 Root-Mean-Square-Error:

The MSE for our practical purposes allows us to compare the “true” pixel values of our original image to our degraded image version. The MSE represents the average of the squares of the “errors” between our actual image and the noisy image. The error is the

amount by which the values of the original image differ from the degraded image. Mean square error is given by:

$$MSE = \frac{\sum_{(i,j)}^N [f(i, j) - F(i, j)]^2}{N^2} \quad RMSE = \sqrt{MSE} \quad (4.3)$$

where  $f$  is the original image and  $F$  is the de-noised image and  $N$  is the size in pixel of the image.

#### 4.3.4 Peak-Signal-to-Noise-Ratio

The PSNR gives the ratio between possible power of a signal and the power of corrupting noise present in the image. The term peak signal-to-noise ratio is an expression for the ratio between the maximum possible value (power) of a signal and the power of distorting noise that affects the quality of its representation. Because many signals have a very wide dynamic range, (Ratio between the largest and smallest possible values of a changeable quantity) the PSNR is usually expressed in terms of the logarithmic decibel scale. The dimensions of the correct image matrix and the dimensions of the degraded image matrix must be identical. PSNR is defined as:

$$PSNR = 20 \log_{10} ((MAX)^2 / MSE), \quad (4.4)$$

where  $MAX$  represents the maximum signal value that exists in our original image. The higher the PSNR is the lower the noise in the image is, which implies a higher image quality image.

#### 4.3.5 Image Contrast Changes

Image contrast is the percentage of intensity changes in global image contrast,  $\Delta C$ . Contrast changes caused by filtering is defined as: the difference in mean intensity between the myocardial and blood pool regions, which is calculated as follows:

$$\Delta C = \left[ \frac{\mu_f^{my} - \mu_f^{bp}}{\frac{1}{N} \sum_{i=1}^N (\mu_i^{my} - \mu_i^{bp})} - 1 \right] * 100, \quad (4.5)$$

where  $\mu_f^{my}$  and  $\mu_f^{bp}$  denote the mean intensity value in the manually selected myocardial and blood-pool regions after filtering respectively;  $\mu_i^{my}$  and  $\mu_i^{bp}$  denote the mean intensity before filtering, the value  $N$  represents the total number of source single-view images;  $m$  represents the  $i^{th}$  image and  $f$  denotes the filtered image.

#### 4.3.6 Contrast-to-Noise-Ratio:

The percentage change in CNR,  $\Delta CNR$ , caused by filtering is defined as:

$$\Delta CNR = \left[ \frac{CNR_f}{\frac{1}{N} \sum_{m=1}^N CNR_i} - 1 \right] * 100, \quad (4.6)$$

whereas the CNR for the filtered image (f) or the  $m^{th}$  single-view image is computed as:

$$CNR = \frac{\mu^{my} - \mu^{bp}}{\sqrt{(\sigma^{my})^2 + (\sigma^{bp})^2}}, \quad (4.7)$$

where  $\sigma$  denotes the standard deviation in the image region.

## 4.4 Comparison Between the Four Algorithms

We will now take a look at the results of the variation of these metrics for the four filters presented in this thesis. For the purpose of performance evaluation, we only consider a region of interest of size 6x5 in both the myocardial and blood pool region for the SNR, Contrast changes, and CNR values as shown in the Figure 4.15. One can see in Table 4.1 the estimated RMSE, PSNR, SNR, Contrast, and CNR of the region of interest without filtering. Table 4.3 and Table 4.4 show the same metrics for the Gaussian filter and the median filters for various  $\sigma$  and window size values. As expected most metrics deteriorate as a function of  $\sigma$  for the Gaussian filter case and as a function of window size for the median filter case. This is due to the fact that the filters cannot adapt to local variation common when speckle noise is present.

Contrary to those two simpler filters, the anisotropic filters: diffusion-gradient based filter and the geodesic filter both have much better performance. One can see in Table 4.5 and Table 4.6 the evolution of the various metrics as a function of the filter parameters. One key observation in both cases is that the SNR increases significantly with those two filters. The SNR almost double in both cases which is an indication that speckle noise is

indeed reduced. The PSNR remains constant relative to the original image for the geodesic filter and is slightly higher for the diffusion-gradient filter for large Kappa values. The key differentiator between the two filtering algorithms is that the contrasts and the RMSE values are improved continuously with  $\sigma$  in the case of the geodesic filter, starting from 34.7 for the original image to 37.7, for  $\sigma = 7$ . The results indicate an excellent increase in contrast and a good reduction of the speckle noise level which is what we were trying to solve. Overall, the geodesic filter behave in a similar way as the well known diffusion-gradient filter but with slightly better results for contrast and the reduction of speckle noise. We also consider a comparison of Gaussian and Geodesic filter approaches for a window size = 11x11, as seen in Table 4.3 and Table 4.7, we notice that as the window size increases, there is a decline in the reduction of speckle noise and the filters perform poorly in these cases.

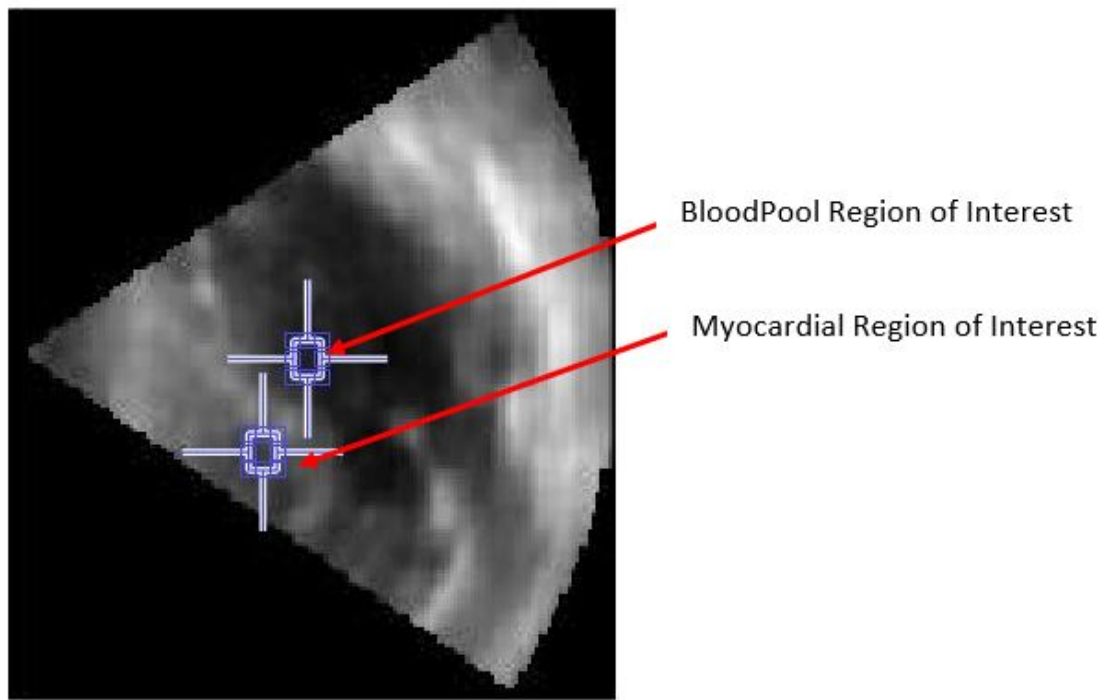


Figure 4.21: Image showing region of interest for performing quantitative measurement analysis.

Table 4.1: *Metrics values for noisy image*

<b>RMSE</b>	<b>PSNR</b>	<b>SNR</b>	<b>Contrast</b>	<b>CNR</b>
34.7870	17.3025	2.0917	1.771	0.0047

Table 4.2: *Metrics values for Gaussian filtering with variable sigma; window size = 3x3*

<b>Parameter - Sigma</b>	<b>RMSE</b>	<b>PSNR</b>	<b>SNR</b>	<b>Contrast</b>	<b>CNR</b>
$\sigma = 1.5$	36.1661	16.9648	1.4149	2.0682	0.0035
$\sigma = 2$	37.5478	16.6391	1.1567	2.1555	0.0030
$\sigma = 2.5$	38.5541	16.4097	0.9680	2.2595	0.0027
$\sigma = 3$	39.5957	16.1778	0.8944	2.4290	0.0024
$\sigma = 5$	43.3435	15.3923	0.4351	3.1615	0.0013

Table 4.3: *Metrics values for Gaussian filtering with variable sigma; window size = 11x11*

<b>Parameter - Sigma</b>	<b>RMSE</b>	<b>PSNR</b>	<b>SNR</b>	<b>Contrast</b>	<b>CNR</b>
$\sigma = 1.5$	41.9413	15.6780	0.0074	0.0197	1.1704e-05
$\sigma = 2$	41.9489	15.6764	0.0100	0.0213	1.2392e-05
$\sigma = 2.5$	41.9665	15.6728	0.0119	0.0219	1.2953e-05
$\sigma = 3$	41.9644	15.6732	0.0138	0.0226	1.3176e-05
$\sigma = 5$	41.9916	15.6676	0.0162	0.0236	1.3311e-05

Table 4.4: *Metrics values for Median filtering with variable window size.*

<b>Parameter - Window</b>	<b>RMSE</b>	<b>PSNR</b>	<b>SNR</b>	<b>Contrast</b>	<b>CNR</b>
3x3	25.7879	19.9025	1.6491	1.9239	0.0040
5x5	26.0949	19.7997	1.3072	2.0867	0.0033
7x7	26.6714	19.6099	1.1437	2.2495	0.0029
9x9	27.0229	19.4962	0.9793	2.3686	0.0026
11x11	29.3685	18.7732	0.8203	2.4483	0.0023

Table 4.5: *Metrics values for Anisotropic Diffusion - gradient based with variable parameters.*

<b>Parameter</b>	<b>RMSE</b>	<b>PSNR</b>	<b>SNR</b>	<b>Contrast</b>	<b>CNR</b>
delta.t = 0.04	33.2431	17.6968	4.5346	1.8828	0.0064
delta.t = 0.09	33.4483	17.6433	4.4778	1.9642	0.0062
delta.t = 0.12	33.1332	17.7255	3.9847	2.0305	0.0057
Kappa = 20	31.9181	18.0501	3.9847	2.0305	0.0057
Kappa = 40	31.9181	18.0589	3.9847	2.0305	0.0057
Kappa = 60	31.9997	18.0279	3.9847	2.0305	0.0057

Table 4.6: *Metrics values for Anisotropic Geodesic with variable sigma; window size = 3x3*

<b>Parameter</b>	<b>RMSE</b>	<b>PSNR</b>	<b>SNR</b>	<b>Contrast</b>	<b>CNR</b>
$\sigma = 1.5$	35.5443	17.1154	4.4659	2.0808	0.0059
$\sigma = 2$	36.5636	16.8698	3.9210	2.2084	0.0054
$\sigma = 3$	37.0061	16.7653	3.7597	2.3980	0.0049
$\sigma = 5$	37.4865	16.6533	3.6804	2.4517	0.0047
$\sigma = 7$	37.7554	16.5912	3.3045	2.4903	0.0044

Table 4.7: *Metrics values for Anisotropic Geodesic with variable sigma; window size = 11x11*

<b>Parameter - Sigma</b>	<b>RMSE</b>	<b>PSNR</b>	<b>SNR</b>	<b>Contrast</b>	<b>CNR</b>
$\sigma = 1.5$	69.6933	11.2670	0.0709	0.0197	2.9030e-05
$\sigma = 2$	69.7071	11.2653	0.0826	0.256	2.9264e-05
$\sigma = 3$	69.7489	11.2591	0.0934	0.0351	2.3183e-05
$\sigma = 5$	69.8362	11.2123	0.1172	0.389	2.3353e-05
$\sigma = 7$	69.9421	11.1948	0.2321	0.4371	2.3721e-05

# Chapter 5

## Conclusion and Future Work

In this thesis, we were able to demonstrate that by adapting a non-linear filter developed to process range images, we were able to filter multiplicative noise in ultrasound images. This new filter called anisotropic geodesic filter possess similar quality as the well-known anisotropic gradient-based filter from Perona-Malik but do not require to compute image gradients and is free of non-intuitive parameters like integration time and diffusion coefficient  $\kappa$ . The filter can be easily generalized to any complex signals such as color range images, MRI, CT etc. One of the key property of this algorithm is its ability to filter continuous regions without the loss of localization of important features. This is a key property for medical applications. The filter is akin to a Gaussian filter in continuous regions and responds like an anisotropic filter in regions with sharp discontinuities. Experimental comparisons with three of the most well-known filters were able to demonstrate its superior capability at filtering ultrasound images.

This filter has numerous potential applications in medical imaging and image processing. Its applications are not just limited to medical and medicine field but can also be used to suppress speckle noise from SAR images as well. In case of ultrasound, it can be used to improve surgical guidance and robotic-assisted interventions which necessitate high quality images where the filtering can be embedded directly in the ultrasound machine.

### 5.1 Future Work

The proposed filter is application specific and can be further generalized for different types of imaging applications. For instance:

- Instead of using a 2-D manifold immersed in an N-D space one could easily generalize the approach to a 3-D or even 4-D manifold immersed in an N-D space. This will allow to process volumetric not only at the slice level but truly at the voxel level for the 3-D case and time varying voxels in the 4-D case;
- Using this framework, one could filter not only CT and MRI but also, with a 4-D framework, real-time cardiac MR data;
- This would require to generalize our Single Source Shortest Path (SS-SP) algorithm to the 3-D and 4-D cases;
- Real-time implementation of the SS-SP algorithm using GPU could be done in order to achieve real-time performance;
- Other medical imaging modalities such as CT, MRI and multi-view ultrasound can be incorporated by applying the filter as a preprocessing step to smooth out 2-D and 3-D images while preserving the fine features of the image such as edges;
- The method can be further extended to multi-spectral images.

# Bibliography

- [1] Hong Minh Cung, Paul Cohen, and Pierre Boulanger. Multiscale edge- and region-based segmentation of range images. *Proc. SPIE 1297, Hybrid Image and Signal Processing II*, September 1990.
- [2] P. Perona and J. Malik. Scale-space and edge detection using anisotropic diffusion. *IEEE Computer Society, IEEE Trans. Pattern Anal. Mach. Intell.*, Vol 12(7):pp. 629–639, July 1990.
- [3] Ana M. Franceschi and Andrew B. Rosenkrantz. Patterns of recent national institutes of health (nih) funding to diagnostic radiology departments. *Academic Radiology*, pages 1076–6332, 2017.
- [4] T. Loupas, W. McDicken, and P. L. Allan. An adaptive weighted median filter for speckle suppression in medical ultrasonic images. *IEEE Trans. Circuits Syst.*, Vol 36(1):pp. 129–135, July 1989.
- [5] X. Zong, A.F. Laine, and E.A. Geiser. Speckle reduction and contrast enhancement of echocardiograms via multiscale nonlinear processing. *IEEE Trans. Med. Imag.*, 17:532–540, Aug 1998.
- [6] P. Courmontagne. Speckle noise reduction: a review advances in seafloor-mapping sonar. *IEEE IM2NP / ISEN-Toulon, France*, Dec.
- [7] David L. Donoho and Iain M. Johnstone. Adapting to unknown smoothness via wavelet shrinkage. *Journal of the American Statistical Association*, 90(432):1200–1224, 1995.
- [8] D. T. Kuan, A. A. Sawchuk, and P. Chavel T. C. Strand. Adaptive noise smoothing filter for images with signal-dependent noise. *IEEE Transactions on Pattern Analysis and Machine Intelligence*, PAMI-7:165–177, 1985.
- [9] J.S. Lee. Digital image enhancement and noise filtering by use of local statistics.
- [10] A. Lopes, E. Nezry, R. Touzi, and H. Laur. Structure detection and statistical adaptive speckle filtering in sar images. *Int. J. Remote Sensing*, 14:1735–1758, 1993.
- [11] V. S. Frost, J. A. Stiles, K. S. Shanmugan, and J. C. Holtzman. Model for radar images and its application to adaptive digital filtering of multiplicative noise. *IEEE Transactions on Pattern Analysis and Machine Intelligence*, PAMI-4:157–166, 1982.
- [12] S. Bannour M. R. Azimi-Sadjadi. Two-dimensional adaptive block kalman filtering of sar imagery. *IEEE Trans. Geosci. and Remote Sensing*, 29:742–753, 1991.
- [13] T. R. Crimmins. Geometric filter for speckle reduction. *Appl. Optics*, 24:1438–1443, 1985.

- [14] A. J. Rye C. J. Oddy. Segmentation of sar images using a local similarity rule. *Pattern Recognition Letters*, 1:443–449, 1983.
- [15] S. Fini L. Alparone, F. Boragine. Parallel architectures for the postprocessing of sar images. *SPIE Proc. #1360, PAMI-4:790–802*, 1990.
- [16] Si Wang, Ting-Zhu Huang, Xi-Le Zhao, Jin-Jin Mei, and Jie Huang. Speckle noise removal in ultrasound images by first- and second-order total variation. *Numerical Algorithms*, Aug 2017.
- [17] A.C. Bovik. On detecting edges in speckle imaginary. *IEEE Trans. Signal Processing.*, 46:1618–1627, Oct 1988.
- [18] A. Lopes, E. Nezry, R. Touzi, and H. Laur. Maximum a posteriori speckle filtering and first order texture models in sar images. In *10th Annual International Symposium on Geoscience and Remote Sensing*, pages 2409–2412, May 1990.
- [19] R. Czerwinski, Douglas L. Jones, , and William D. OBrien. Detection of lines and boundaries speckle images application to medical ultrasound. *IEEE Trans. on Medical Imaging*, 18(2), Feb 1999.
- [20] N K Ragesh, A.R Anil, and R. Rajesh. Digital image denoising in medical ultrasound images: a survey. *ICGST AIML-Conference*, Vol 11:pp. 12–14, 2011.
- [21] S. Hariharasudhan and Dr.B. Raghu. *A Virtual Analysis on Effective Speckle Noise Removal Techniques in Medical Images by Various Filtering Methods*, volume V38(3). Seventh Sense Research Group, 2016.
- [22] Anil K. Jain. *Fundamentals of Digital Image Processing first edition*. Prentice Hall, Inc, 1989.
- [23] D.T. Kaun, A.A. Sawchuk, T.C. Strand, and P.Chavel. Adaptive noise smoothing filter for images with signal dependent noise. *IEEE Trans. Pattern Analysis and Machine Intelligence*, Vol 2:pp. 165–177, March 1985.
- [24] Shi Zhenghao and B.Fung Ko. *A comparison of digital speckle filters*. Canada Center for Remote Sensing.
- [25] Y. Luo, C. Tao, X. Qiang, and Zeng X. Denoising by anisotropic diffusion of independent component coefficients. *Lecture Notes in Computer Science, Neural Information Processing*, pages 1117–1124, 2006.
- [26] O.V Michailovich and A. Tannenbaum. Despeckling of medical ultrasound images. *IEEE transactions on ultrasonics, ferroelectrics, and frequency control*, Vol 53, 2006.
- [27] CB. Burckhardt. Speckle in ultrasound b-mode scans. *IEEE Trans. Sonics Ultrason.*, SU-25:1–6, Jan 1978.
- [28] R.R. Coifman and D.L. Donoho. Translation invariant denoising in wavelets and statistics. *Springer Lecture notes in Statistics, 103, springer-Verlang.*, pages 125–150, 1994.
- [29] D.L. Donoho and I.M. Johnstone. De-noising by soft-thresholding. *IEEE Trans. on Information Theory*, Vol 17(3), 1995. :613-27.
- [30] Rafael C. Gonzalez and Richard E. Woods. *Digital Image Processing*. 2nd Edition Prentice Hall, Inc, Upper Saddle River, NJ, 2002.

- [31] S. Mallat. A theory of multiresolution signal decomposition: The wavelet representation. *IEEE Trans. Pattern Anal. Machine Intell.*, 11:674–693, July 1989.
- [32] J.S. Lee. Speckle analysis and smoothing of synthetic aperture radar images. *Comp. Graphics Image Processing*, 17:24–32, Aug 1981.
- [33] Y. Yongjian and S.T. Acton. Speckle reducing anisotropic diffusion. *IEEE Trans. Image Processing*, 11(11):1260–1270, Nov. 2002.
- [34] J.W. Godman. Some fundamental properties of speckle. *Jl. Opt. Soc. Am.*, 66(11):1145–1149, 1976.
- [35] Paul Suetens. *Fundamentals of Medical Imaging*. (1st Edition), Cambridge university, UK, 2002.
- [36] W.R. Hedrick and D.L. Hykes. Image and signal processing in diagnostic ultrasound imaging. *Journal of Diagnostic Medical Sonography*, Vol 5(5):231–239, 1989.
- [37] Y. You, W. Xu, A. Tannenbaum, and M. Kaveh. Behavioral analysis of anisotropic diffusion in image processing. *IEEE Trans. Image Processing.*, 5:1539–1553, Nov 1996.
- [38] Palwinder Singh and Leena Jain. Noise reduction in ultrasound images using wavelet and spatial filtering techniques. *IEEE 2nd International Conference on Information Management in the Knowledge Economy.*, pages 57–63, 2013.
- [39] Jean Cousty. *Introduction to grayscale morphology*. MorphoGraph and Imagery, 2011.
- [40] Gyger Cyrill, Cattin Roger, Hasler Pascal W., and Maloca Peter. Three-dimensional speckle reduction in optical coherence tomography through structural guided filtering. *Optical Engineering*, 53(7):53 – 53 – 10, 2014.
- [41] D. A. Nelson Mascarenhas. An overview of speckle noise filtering in sar images. *European Space agency. Provided by the NASA Astrophysics Data System*.
- [42] Y. Huang and J. L. van Genderen. Evaluation of several speckle filtering techniques for ers-1 and 2 imagery. *International Archives of Photogrammetry and Remote sensing.*, 31(B2), 1996.
- [43] S.Kalaivani Narayanan and R.S.D.Wahidabanu. A view on despeckling in ultrasound imaging. *International Journal of Signal Processing, Image Processing and Pattern Recognition*, 2(3), Sept. 2009.
- [44] R. Wagner, Smith, John M. Sandrik, and Lopez. Statistics of speckle in ultrasound b-scans. *IEEE Trans. on Sonics and Ultrasonics*, 3(3), May 1983.
- [45] Y. Yu and Scott T. Acton. Speckle reducing anisotropic diffusion. *IEEE Trans. On Image Processing*, 11, Nov 2002.
- [46] J. Lee. Digital image enhancement and noise filtering by use of local statistics. *IEEE Trans. On Pattern Analysis and Machine Intelligence*, Pami-2(2), March 1980.
- [47] A. Garg, Jyoti Goal, Sandeep Malik, Kavita Choudhary, and Deepika. De-speckling of medical ultrasound images using wiener filter and wavelet transform. *International Journal of Electronics and Comm. Technology*, 2(3), Sept 2011.

- [48] K. Kaur, Baljit Singh, and Mandeep Kaur. Speckle noise reduction using 2-d fft in ultrasound images, speckle noise reduction filters on active radar and sar images. *International Journal of Advances in Engineering and Technology*, Sept 2012.
- [49] *Techniques: A Comparative Approach*, volume 2. International Journal of Scientific Engineering and Research (IJSER).
- [50] Asoke Nath. Image denoising algorithms: A comparative study of different filtration approaches used in image restoration. *IEEE Xplore*, page 157–163, 2013.
- [51] Khalifa Dejmal. Speckle reduction in ultrasound images by minimization of total variation. *IEEE*, 3:375–60, 2005.
- [52] W.K. Prat. *Digital Image Processing*. Wiley, NY, 1978.
- [53] Mark S. Nixon and Alberto S. Aguado. *Feature Extraction and Image Processing*. Newnes, 2002.
- [54] K. Thangavel, R. Manavalan, and I. Laurence Aroquiaraj. Removal of speckle noise from ultrasound medical image based on special filters: Comparative study. *ICGST-GVIP Journal*, June 2009.
- [55] V.S Frost, J.A Stiles, K.S Shanmugam, and J.C Holtzman. A model for radar images and its application for adaptive digital filtering of multiplicative noise. *IEEE Transactions on pattern analysis and machine intelligence*, 4(2):157–165, 1982.
- [56] D. R. K. Brownrigg. The weighted median filter. *Commun. Assoc. Comput. Mach.*, 27:807–818, Aug 1984.
- [57] T. Loupas. Digital image processing for noise reduction in medical ultrasonic images. *Univ. of Edinburgh*, 1988.
- [58] B. Kawohl and N. Kutev. Maximum and comparison principle for one-dimensional anisotropic diffusion. *Math. Ann.*, 311(1):107–123, 1998.
- [59] S. Kichenassamy. The perona-malik paradox. *SIAM J. Appl. Math.*, 57(5):1328–1342, 1997.
- [60] P. Perona, T. Shiota, and J. Malik. Anisotropic diffusion. geometry-driven diffusion in computer vision. *Computational Imaging and Vision*, 1:73–92, 1994.
- [61] Lewis D. Griffin. *Scale Space Methods in Computer Vision*. 4th International Conference Scale-Space, Springer Science and Business Media, Isle of Skye, UK, June 2003.
- [62] Song Xiao-yang, Chen Ya-zhu, Zhang Su, and Yang Wei. Speckle reduction based on contourlet transform using scale adaptive threshold for medical ultrasound image. *J. Shanghai Jiaotong Univ. (Sci)*, 13(5):553–558, 2008.
- [63] K. Punithakumar, A. R. Hareendranathan, R. Paakkanen, N. Khan, M. Noga, P. Boulanger, and H. Becher. Multiview echocardiography fusion using an electromagnetic tracking system. In *38th Annual International Conference of the IEEE Engineering in Medicine and Biology Society (EMBC)*, pages 1078–1081, Aug 2016.
- [64] Krystyna Malik, Bernadetta Machala, and Bogdan Smolka. Novel approach to noise reduction in ultrasound images based on geodesic paths. In Leszek J. Chmielewski, Ryszard Kozera, Bok-Suk Shin, and Konrad Wojciechowski, editors, *Computer Vision and Graphics*, pages 409–417, Cham, 2014. Springer International Publishing.

- [65] Jing Wu Bianca S. Gerendas Christian Simader Georg Langs Sebastian M. Waldstein Ursula Schmidt-Erfurth Ehsan Shahrian Varnousfaderani, Wolf-Dieter Vogl. Geodesic denoising for optical coherence tomography images, 2016.
- [66] L. Bertelli and B. S. Manjunath. Edge preserving filters using geodesic distances on weighted orthogonal domains. In *2007 IEEE International Conference on Image Processing*, volume 1, pages I – 321–I – 324, Sept 2007.
- [67] Jacopo Grazzini and Pierre Soille. Edge-preserving smoothing using a similarity measure in adaptive geodesic neighbourhoods. *Pattern Recogn.*, 42(10):2306–2316, October 2009.

# Appendix A

## Matlab Code For 3D Geodesic Filter

---

```
%% -----  
%% This function reads the 3D Volume - HDR Image and performs  
%% Anisotropic Geodesic Filter on the 3D Volume  
%% -----  
function GeodesicUS3D()  
  
clear all ; clc ; close all  
  
% Get image(s) from the user  
function [dim, sp] = read_hdr_header(fname)  
    % read the header information  
    fid = fopen(fname);  
    dim = sscanf(fgets(fid), '%d'); % dimension of the 3D volume  
    sp = sscanf(fgets(fid), '%f'); % spacing in x, y, z directions  
    fclose(fid);  
end  
  
function vol_data = read_binary_file(fname, dim)  
    % read binary image file  
    fileID = fopen(fname);  
    vol_data = reshape(fread(fileID, 'uint8'), dim); % reshape the  
        array into 3D volume  
    fclose(fileID);  
end  
  
[fname, pathname, ~] = uigetfile('*.hdr', 'Select an HDR  
    file'); % get the filename  
fname = fullfile(pathname, fname); % fullpath to the header file  
fbname = [fname(1:end-4) '.img']; % fullpath to the image file  
  
[dim, sp] = read_hdr_header(fname); % read header file  
    information
```

```

vol_data = read_binary_file(fbname, dim); % read corresponding
    volume from binary image

size(vol_data)

% Visualize the 3D Volume
vis3d(vol_data, '', 'Original - 3D Volume');

%% Applying Gaussian Filter to remove Additive Noise
volSmooth = imgaussfilt3(vol_data);

% Visualize the Gaussian Filtered 3D Volume
vis3d(volSmooth, '', 'Gaussian Filtered - 3D Volume');

% Application of Geodesic Filter to an Ultrasound Image

% Perform Anisotropic Geodesic Filter
diff_vol = Geodesic3DFilter(volSmooth);

% Visualize Filtered Volume
vis3d(diff_vol, '', 'Filtered Volume')
end

%% -----
function diff_vol = Geodesic3DFilter(vol_data)

% Design the Kernel
thr_z = 200;
nb_iter = 1;
sigma = 5;

sigma2 = sigma*sigma;

% Define the Window Size
WL = 3;
WC = WL;
WS = WL;

% Define x y z
size_vol = size(vol_data);
lines = size(vol_data,1);
columns = size(vol_data,2);
slices = size(vol_data,3);

[x, y, z] = meshgrid(1:columns, 1:lines, 1:slices);

M = (WL - 1) / 2;

```

```

N = (WC - 1) / 2;
P = (WS - 1) / 2;
%% -----

% Convert input volume to double.
vol_data = double(vol_data);

% Start the Convolution
for iter = 1:nb_iter
    fprintf('Iteration Number : %d\n', iter)

    fprintf('Start Convolution... \n')
    % Calculate the Geodesic 3D Filter - Filter Implementation
    for i = 1+M : lines-M
        for j = 1+N : columns-N
            for k = 1+P : slices-P

                %Extract the voxel window
                for l = -M : M
                    for m = -N : N
                        for n = -P:P
                            wind(l+M+1, m+N+1, 1) = x(i+1, j+m, k+n);
                            wind(l+M+1, m+N+1, 2) = y(i+1, j+m, k+n);
                            wind(l+M+1, m+N+1, 3) = z(i+1, j+m, k+n);
                        end
                    end
                end
            end
        end
    end
%% -----

% Compute Surface Distances
[dis, ~] = Surface_Dist3D(wind, WL, WC);

sum_weight = 0;
% Compute the convolution kernel
for l = 1 : WL
    for m = 1 : WC
        for n = 1 : WS
            sigma = 1.5;
            sigma2 = sigma*sigma;
            weight(l,m,n) =
                exp(-(dis(l,m).^2)/(2.0*sigma2));
            sum_weight = sum_weight + weight(l,m,n);
        end
    end
end

weighted_avg = zeros(i, j, k);

```

```

    % Do Weighted Average
    for l = 1 : WL
        for m = 1 : WC
            for n = 1: WS
                weighted_avg(i, j, k) = weighted_avg(i, j, k) +
                    weight(l, m, n)*wind(l, m, 2);
            end
        end
    end
end
%%
-----
    % Normalize the results
    sx(i, j, k) = x(i, j, k);
    sy(i, j, k) = y(i, j, k);
    sz(i, j, k) = z(i, j, k);
    weighted_avg(i, j, k) = weighted_avg(i, j, k)/sum_weight;
end
end
end

% Save the results back in x,y and z and compute the variation
with the
% original surface.
var = 0.;
nbv = 0;
diff_vol = zeros(size(vol_data));
for i = 1+M : lines-M
    for j = 1+N : columns-N
        for k = 1+P : slices-P
            var = var + ((sx(i, j, k)-x(i, j, k)).^2 +
                (sy(i, j, k)-y(i, j, k)).^2 +
                (weighted_avg(i, j, k)-z(i, j, k)).^2);
            nbv = nbv+1;
            x(i, j, k) = sx(i, j, k);
            y(i, j, k) = sy(i, j, k);
            z(i, j, k) = weighted_avg(i, j, k);

            Temp = vol_data(i:i+M, j:j+N, k:k+P).*var;
            diff_vol(i, j, k) = sum(Temp(:));
        end
    end
end

var = sqrt(var/(nbv-1));

% Iteration Terminated
fprintf ('Iteration Number : %d terminated\n', iter)

```

```

    fprintf ('Variation between t and t+1 is : %f\n', var)

end
%%
-----
% Compute Intrinsic Surface Distances within the given window by
% Using the Single-Source Shortest Path Algorithm
% INPUT
% Wind(WL,WC,3) : X,Y,Z components of the pixels in the window
% WL, WC : Size of the Window
% OUTPUT
% dis(WL,WC) : Intrinsic surface distances from the center pixel
% Prec(WL,WC,2) : Backward trajectory of geodesic

function [dis, Prec] = Surface_Dist3D(Wind, WL, WC)
Vmax = 1.0e30;
M = (WL-1)/2;
N = (WC-1)/2;

% Initialization of the Heap, SP
for i = -M:M
    for j = -N:N
        icode = iencode(i, j, M, N);
        SP(icode) = Vmax;
        LOC(icode) = icode;
        ELM(icode) = icode;
        MARK(icode) = 0;
    end
end

SP(1) = 0;
icode = iencode(0, 0, M, N);
elm1 = ELM(1);
iloc = LOC(icode);
LOC(icode) = 1;
ELM(1) = icode;
ELM(iloc) = elm1;
LOC(elm1) = iloc;

Prec(M+1, N+1, 1) = 0;
Prec(M+1, N+1, 2) = 0;

for i = 1:(WL*WL-1)
    nrest = WL*WL-i+1;
    % Find the next shortest path
    icodew = ELM(1);
    spw = SP(1);

```

```

[iw, jw] = idecode(icodew, M, N);
% Remove the first element from the heap SP
MARK(icodew) = 1;
sp1 = SP(1);
elm1 = ELM(1);
SP(1) = SP(nrest);
LOC(ELM(1)) = 1;
SP(nrest) = sp1;
ELM(nrest) = elm1;
LOC(elm1) = nrest;
% CALL SHIFT DOWN
shiftdown(SP,1,nrest-1,LOC,ELM);
% First Element is Removed

% Update the shortest distances in the heap, SP
dmin = Vmax;
for ii = -1:1
    for jj = -1:1
        iz = iw + ii;
        jz = jw + jj;
        if (-M <= iz <= M) && (-N <= jz <= M)
            icodez = iencode(iz, jz, M, N);
            elseif (MARK(icodez) == 0)
                spz = SP(LOC(icodez));
                dist = edge_length(iw+M+1, jw+N+1, iz+M+1, Wind);
            elseif((spw + dist)< spz)
                % The distance is less than the current distance,
                % So update the heap
                SP(LOC(icodez)) = spw + dist;

% CALLING SHIFTPUP FUNCTION
                shiftpup(SP,LOC(icodez),nrest-1,LOC,ELM);
                Prec(iz+M+1, jz+N+1, 1) = iw + M + 1;
                Prec(iz+M+1, jz+N+1, 2) = jw+ N + 1;
            end
        end
    end
end

% Output the current Distance

for ii = -M:M
    for jj = -N:N
        icode = iencode(ii, jj, M, N);
        dis(ii+M+1, jj+N+1) = SP(LOC(icode));
    end
end
end

```

```

end

for i = -M:M
    for j = -N:N
        icode = iencode(i, j, M, N);
        dis(i+M+1, j+N+1) = SP(LOC(icode));
    end
end
return
end

%% Compute the distance between 2 points (iw,jw) and (iz,jz)

function distance = edge_length(iw, jw, iz, jz, Wind)
d = 0.0;
for i = 1:3
    d = d + (Wind(iw, jw, i) - Wind(iz, jz, i)).^2;
end
distance = sqrt(d);
end

%% Compute linear index of the window
function icode = iencode(I,J,MI,MJ)
icode = (2*MJ+1)*(I+MI)+J+MJ+1;
return
end

%% decode the linear code into index of window
function [I,J] = idecode(icode,MI,MJ)
I=(icode-1)/(2*MJ+1)-MI;
J=icode-(2*MJ+1)*(I+MI)-MJ-1;
return
end

%%
-----
function shiftdown(H,is,ie,LOC,ELM)
% Shiftdown procedure for heap update
% Heap: H(1) is min
%
i = is;
j = 2*i;
x = H(i);
p = ELM(i);
if (j < ie)
    if (j < ie)
        if (H(j) > H(j+1))

```

```

        j = j+1;
    end
end
if (x < H(j))
    H(i) = x;
    H(i)=H(j);
    pp=ELM(j);
    ELM(i)=pp;
    LOC(pp)=i;
    i=j;
    j=2*i;
end
H(i)=x;
LOC(p)=i;
ELM(i)=p;

end
return
end
%%
-----
function shiftup(H,is,ie,LOC,ELM)
% Shiftup procedure for heap update
% Heap: H(1) is min
%

i=is;
j=i/2;
x=H(i);
p=ELM(i);

if (j > 1)
    if (H(j) < x)
        H(i)=H(j);
        pp=ELM(j);
        ELM(i)=pp;
        LOC(pp)=i;
        i=j;
        j=i/2;
    end
    H(i)=x;
    ELM(i)=p;
    LOC(p)=i;
end
return
end
end

```

---